TECHNISCHE UNIVERSITÄT WIEN
Vienna University of Technology

Diplomarbeit

Central Exclusive Production of Pseudoscalar and Axial Vector Mesons through Pomeron Fusion

zur Erlangung des akademischen Grades
Diplom-Ingenieur
im Rahmen des Studiums
Technische Physik

eingereicht von
Florian Hechenberger
Matrikelnummer 1327739

ausgeführt am

Institut für Theoretische Physik der Fakultät für Physik der technischen Universität Wien

unter der Anleitung von
Univ.-Prof. DI Dr. A. Rebhan

....
Unterschrift (Betreuer) Unterschrift (Student)

Wien, am
15. Dezember 2019

Abstract

The central exclusive production of the pseudoscalar and axial vector mesons η' and f_1 is studied in peripheral proton collisions. This process is considered in the Regge limit, i.e. high energy limit with small transverse momentum transfer, which is thought to predominantly produce glueball intermediate states. These intermediate states will be parametrized using Pomeron trajectories. On the one hand vertices and propagators from the Witten-Sakai-Sugimoto model, which is a top-down holographic approach to low-energy Quantum Chromodynamics, is used. On the other hand the Tensor-Pomeron model is used, which is an effective field theory guided by gauge principles and covariance. A comparision of these models is made based on experimental results from the WA102 collaboration.

Contents

Introduction

Due to the non-abelian nature of Quantum Chromodynamics (QCD), the widely accepted theory of the strong interactions, bound states of gauge bosons, so called glueballs, can form. Due to the mixing with mesonic states and their theoretically predicted large masses, the detection of these elusive particles remains a challenging task for ongoing experiments such as BES III [1] as well as future experiments such as PANDA [2] at FAIR. The strong gluon self coupling adds to the difficulty of detecting these particles, as sophisticated calculations are needed for theoretical predictions. Among lattice computations and chiral perturbation theory, a more recent model has been proposed by Sakai and Sugimoto [3] which is a top-down holographic approach to QCD based on work by Witten [4]. In the Witten model an AdS/CFT like correspondence between type-IIA supergravity, which is essentially a low energy limit of string theory, and pure glue superconformal Yang-Mills (YM) theory is established. Supersymmetry is then broken similar to finite temperature effects which lead to the different distribution functions of bosons and fermions. The breaking of conformal invariance is achieved by a stack of N_c D4-branes in AdS space on the supergravity side. The low energy limit of this theory is then dual to large N_c YM theory in four dimensions. Sakai and Sugimoto then added pairs of $D8$ and $\overline{D8}$ branes intersecting with the $D4$ brane to account for flavour symmetry and hence introduce chiral quarks. This model can then be used to calculate effective Lagrangians including mesons as well as glueball states and their interactions, from which one can calculate decay rates and cross sections involving glueballs [5, 6].

This work is structured as follows: In chapter 1 theoretical as well as experimental aspects of glueballs are briefly reviewed and some experiments dealing with central exclusive production (CEP) are described. In chapter 2 the necessary theoretical models are reviewed. Chapter 3 deals with the parametrization of the phase space and the calculations of the differential cross sections used in CEP. Chapter 4 comprises conclusions and an outlook for future work. The appendices B, C and D contain additional information on the axial anomaly, the Tensor-Pomeron model and the Witten-Sakai-Sugimoto model, respectively.

Chapter 1

Prerequisites

In the following chapter the concept of Glueballs is introduced and a short historical overview for the search of these particles is given. Furthermore the WA102 experiment is described which provided the data for the fitting procedure in chapter 3.

1.1 Glueballs

For a comprehensive review on glueballs and mesons see [7].
Due to the non-abelian structure of the strong interactions

$$\begin{aligned} \mathcal{L}_{QCD} &= \bar{\psi}_i \left(i(\gamma^\mu D_\mu)_{ij} - m\delta_{ij} \right) \psi_j + \mathcal{L}_{YM} \\ \mathcal{L}_{YM} &= -\frac{1}{4} G^a_{\mu\nu} G^{\mu\nu a} \\ G^a_{\mu\nu} &= \partial_\mu A^a_\nu - \partial_\nu A^a_\mu + g f^{abc} A^b_\mu A^c_\nu, \end{aligned} \tag{1.1}$$

gluons too carry color charge and theoretically should be able to form bound states: Glueballs. However calculating these states proves quite cumbersome due to the coupling constant of the strong interaction being quite large ($\alpha_s(1\text{GeV}) \approx 0.5$ in the $\overline{\text{MS}}$ scheme) at low energies where bound states are prominent.

There are many ways to describe glueballs and other bound states using first principles on the one hand

- Lattice QCD:
  In lattice simulations spacetime is discretized with some lattice constant and correlation functions are calculated using the partition function, i.e. path integral [8].

- Bethe-Salpeter Equations:
  The pole of the two-particle Green's function constructed from the Bethe-Salpeter wave function $\Psi = \langle\Omega| \phi_1\phi_2 |\psi\rangle$, is identified with a bound state. The wave function parametrizes a transition amplitude from the constituent states ϕ_i to the bound state ψ. Using the Dyson equation for the two-particle Green's function, one then calculates the Bethe-Salpeter wave function [9].

- Holographic QCD:
  The AdS/CFT correspondence is used to map QCD to a higher-dimensional AdS space. The strongly coupled regime of QCD thus becomes weakly coupled in the dual theory [10].

and effective theories on the other

- Linear Sigma Model:
  An effective Lagrangian, which incorporates colour, chiral, CPT and dilatation symmetry for the meson multiplets is constructed. Dilatation symmetry is then explicitly broken and a shift in the dilaton field around its classical value gives rises to a particle which can be identified with a scalar glueball [11].

- Chiral Perturbation Theory (χPT):
  An effective Lagrangian, which is consistent with all the symmetries of QCD, is constructed using the Goldstone bosons of the spontaneous breaking of the approximate chiral symmetry. Using this Lagrangian a perturbative expansion in even powers of the momenta $\mathcal{O}(p^2)$ is then performed to calculate physical observables [12].

just to name a few.

In Ref.[13] Morningstar and Peardon calculated the glueball spectrum of pure $SU(3)$ gauge theory using lattice simulations. The results of a more recent lattice calculation are shown in figure 1.1. This spectrum has also been obtained using the Bethe-Salpeter equations [14].

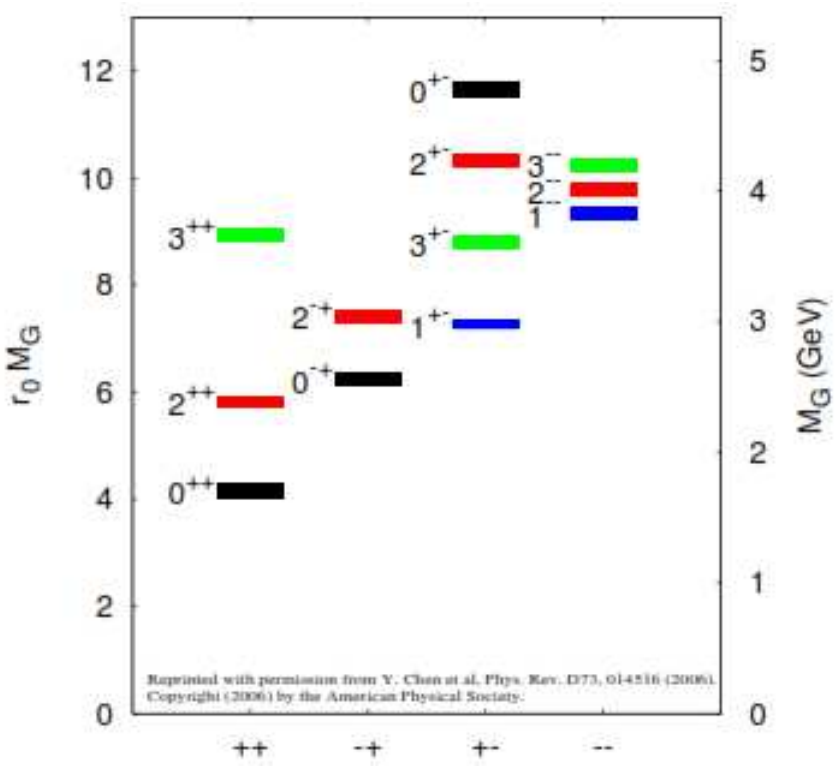

Figure 1.1: Glueball spectrum from [15] of pure $SU(3)$ gauge theory. r_0 is the hadronic scale assumed to be $r_0^{-1} = 410$ MeV. The height of each box corresponds to the statistical uncertainty in the masses.

1.2 The WA102 experiment

Built in 1995 the WA102 experiment was searching for non $q\bar{q}$ states predicted by QCD, those of particular interest for the collaboration are given in table 1.1.

$gg,\ ggg$	Glueballs
$q\bar{q}g$	Hybrids
$q\bar{q}q\bar{q}$	Tetraquarks

Table 1.1: Some non $q\bar{q}$ states

Due to their short lifetimes and mixing with $q\bar{q}$ states, searching for glueball states is not an easy task. Promising approaches:

- Search for Oddballs
  States with J^{PC} not allowed for $q\bar{q}$ states
- Search for extra states
  States with quantum numbers of an already completed nonet
- Search for states with unusual branching ratios
- Search for states preferentially produced in gluon rich processes (e.g. double pomeron exchange, see figure 1.2)

Previous searches in the experiments WA76 (1982), WA91 (1994) and NA12/2 (1986) have studied exclusive final states with a presumed strong gluonic component in the reactions

$$\begin{aligned} pp &\to p_f p_s(X^0) \\ \pi^+ p &\to \pi^+_f p_s(X^0) \end{aligned} \tag{1.2}$$

where the subindices denote fast and slow states respectively. The reaction is depicted in figure 1.2.

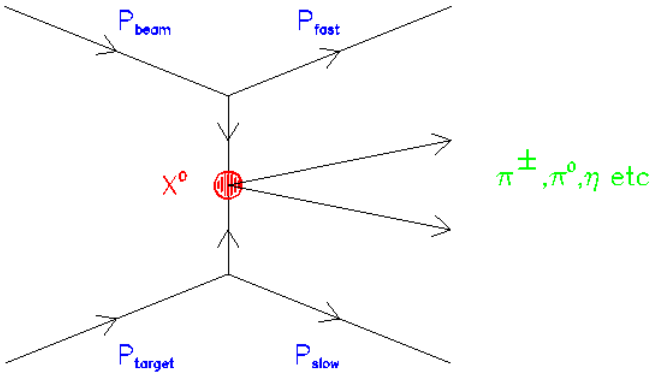

Figure 1.2: Center of momentum (CM) frame view of the reactions 1.2. Image taken from [16]

The WA102 experiment aimed to combine the best of WA76, WA91 and NA12/2 which all found evidence for non $q\bar{q}$ states. A main goal was the search for η and η' mesons which were assumed to be prefered states from glueball decays.

1.2.1 Setup

The setup of the experiment is depicted in figure 1.3. The experiment uses beam momenta of 450 GeV/c and center of mass energies of $\sqrt{s} = 29.1$ GeV and the charged particle reconstruction of the CERN Omega Spectrometer combined with the multiphoton detection of the GAMS 4000 electromagnetic calorimeter.

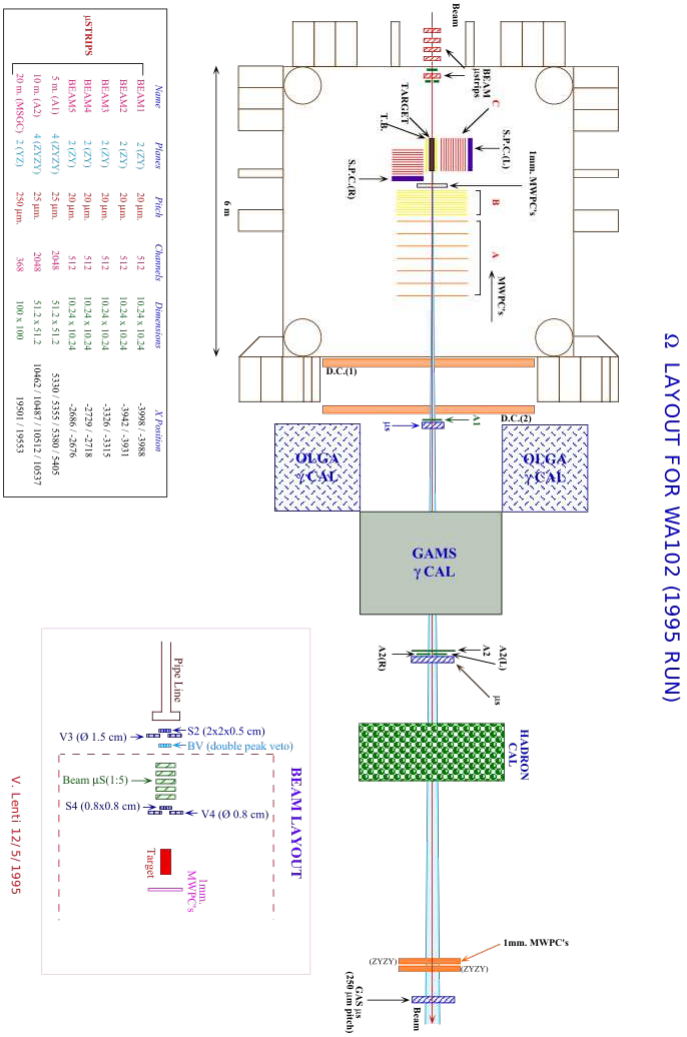

Figure 1.3: Setup of the WA102 experiment in 1995 from [17]

For additional information on the experiments WA76, WA91 and WA102 see [18].

Chapter 2

Overview of theoretical models

The following chapter gives a quick introduction to the models and techniques which where used in the calculations of chapter 3.

2.1 Regge theory

In Regge theory analytical properties of the S-matrix are used to parametrize amplitudes of elastic processes in terms of total angular momentum. It is found that the masses of bound state particles lie on so-called Regge trajectories that are usually assumed to be linear and which are in good agreement with experimental observations. The idea is that in certain processes not only single particles are exchanged during the scattering event but rather whole towers of particles with increasing spin that couple like the lowest lying spin component.

For a detailed discussion see [19] or [20].

2.1.1 Dispersion relations

Recall the optical theorem which states that the total cross section for a $2 \to 2$ process is given by the imaginary part of the elastic forward scattering amplitude $A(s, t = 0)$

$$\sigma_{12}^{tot} = \frac{1}{2|\mathbf{p}|\sqrt{s}} \mathrm{Im} A(s, t = 0). \tag{2.1}$$

This result can be derived from unitarity conditions of the S-matrix. In particular from

$$\delta_{ji} = \langle j | S^\dagger S | i \rangle , \quad S = 1 + iT \tag{2.2}$$

follows

$$\langle j|\,T\,|i\rangle - \langle j|\,T^\dagger\,|i\rangle = (2\pi)^4 i \sum_f \delta^4(P^f - P^i)\,\langle j|\,T^\dagger\,|f\rangle\,\langle f|\,T\,|i\rangle\,. \tag{2.3}$$

Under the assumption that bound states correspond to poles and branch points with cuts attached correspond to physical thresholds of the amplitude, crossing relations between Mandelstam variables can be formulated. Using this crossing symmetry one can analytically continue one amplitude to another. For example

$$A_{a+b\to c+d}(s,t,u) = A_{a+\bar{c}\to\bar{b}+d}(t,s,u) = A_{a+\bar{d}\to\bar{b}+c}(u,t,s). \tag{2.4}$$

Using analytic continuation and the Schwarz reflection principle, the complex conjugate of the physical amplitude can be obtained. This can be used to calculate the imaginary part of the amplitude

$$2i\,\mathrm{Im}\,A(s+i\epsilon,t) = A(s+i\epsilon,t) - A(s-i\epsilon,t) = D_s(s,t,u). \tag{2.5}$$

The quantity $D_s(s,t,u)$ is called the s-channel discontinuity. The discontinuities for t- and u-channel are defined equivalently.
Now, using the analyticity and that the amplitude tends to zero sufficiently quickly as $|s|\to\infty$, Cauchy's theorem can be used to write

$$A(s,t) = \frac{g_s^2}{s-s_B} + \frac{g_u^2}{u-u_B} + \frac{1}{2\pi i}\int_{s_0}^{\infty} \mathrm{d}s' \frac{D_s(s',t,u')}{s'-s} + \frac{1}{2\pi i}\int_{u_0}^{\infty} \mathrm{d}u' \frac{D_u(s',t,u')}{u'-u} \tag{2.6}$$

where g_s and g_u are the residues of the corresponding poles at s_B and u_B that lie below the thresholds s_0 and u_0, respectively. Including bound states below the threshold by defining

$$D_s(s,t,u) = -2\pi g_s^2 \delta(s-s_B), \qquad s < s_0 \tag{2.7}$$

further simplifies the amplitude to

$$A(s,t) = \frac{1}{2\pi i}\int_0^{\infty} \mathrm{d}s' \frac{D_s(s',t,u')}{s'-s} + \frac{1}{2\pi i}\int_0^{\infty} \mathrm{d}u' \frac{D_u(s',t,u')}{u'-u} \tag{2.8}$$

If the amplitude does not tend to zero sufficiently fast for large values of s, one can make subtractions of higher powers of s and write instead

$$\begin{aligned} A(s,t) - A(s_1,t) &= \frac{1}{2\pi i}\oint \mathrm{d}s' A(s',t)\left(\frac{1}{s'-s} - \frac{1}{s'-s_1}\right) \\ &= \frac{s-s_1}{2\pi i}\oint \mathrm{d}s' \frac{A(s',t)}{(s'-s)(s'-s_1)} \end{aligned} \tag{2.9}$$

Equation (2.8) is called a dispersion relation and (2.9) a once subtracted dispersion relation. It it possible to generealize this procedure to an arbitrary number of subtractions in order for the integral in (2.8) to converge. See e.g. [19] or [20] for an in depth discussion of this procedure.

2.1.2 Partial-wave amplitudes

For typical scattering processes in the CM frame the momentum transfer t varies linearly with $z_s = \cos\theta_s$, with θ_s being the s-channel scattering angle. Hence $t = t(s, z_s)$ and the amplitude where the spin states are ignored can be expanded in a partial wave series

$$A(s, t(s, z_s)) = 16\pi \sum_{l=0}^{\infty} (2l+1) A_l(s) P_l(z_s), \tag{2.10}$$

where the P_l are the Legendre polynomials of the first kind and A_l is call the partial-wave amplitude and given by

$$A_l(s) = \frac{1}{16\pi} \frac{1}{2} \int_{-1}^{+1} \mathrm{d}z_s . P_l(z_s) A(s, t(s, z_s)). \tag{2.11}$$

Each of these partial-wave amplitudes satisfies its own unitarity equation (see e.g. [20] for details) and can be written as

$$A_l(s) = \frac{\eta_l(s) e^{2i\delta_l(s)} - 1}{2i\rho(s)}, \tag{2.12}$$

where $0 < \eta_l \leq 1$ is the inelasticity, δ_l a (real) phase shift and the partial wave phase-space factor $\rho = 2|\mathbf{p}|\sqrt{s}$. Sometimes it is useful to define δ_l as a complex variable and write using $\eta_l = e^{-2\,\mathrm{Im}(\delta_l)}$

$$A_l(s) = \frac{e^{2i\delta_l(s)} - 1}{2i\rho(s)}. \tag{2.13}$$

The series (2.10) cannot converge for all values of s, t and u. For example for physical values of s it must diverge at the nearest t or u singularity, since all of the arguments above are footed on crossing symmetry. The t and u channel poles lie beyond the physical region of t and u, i.e. $|z_s| > 1$. However, it can be shown that the series converges within an ellipse [21] in the complex z_s plane where the foci are located at $z_s = \pm 1$. This and the Legendre polynomials of the second kind $Q_l(z)$, with branch cuts at $z = \pm 1$ for physical values of l, can be used to write

$$A_l(s) = \frac{i}{32\pi^2} \oint \mathrm{d}z_s Q_l(z_s) A(s, t(s, z_s)). \tag{2.14}$$

Since $Q_l(z) \sim z^{-l}$ for sufficiently large values of z, the contour can be closed at infinity and Chauchy's theorem can be used. Discarding the singularities at infinity and using the disontinuities D_t and D_u (see equation 2.5) gives

$$A_l(s) = \frac{1}{32i\pi^2} \left(\int_1^\infty \mathrm{d}z'_s D_t(s, t(s, z'_s)) Q_l(z'_s) + \int_{-1}^\infty \mathrm{d}z'_s D_u(s, u(s, z'_s)) Q_l(z'_s) \right), \tag{2.15}$$

which is known as the Froissart-Gribov projection. This notion of analytic continuation will later be used to introduce the concept of complex angular momentum and ultimately Regge theory.

2.1.3 Regge poles and complex angular momentum

Using the parity of the Legendre polynomials $P_l(-z) = (-1)^l P_l(z)$ one can rewrite the t-channel partial wave series (2.10) using

$$A_l(s, t) = A_l^+(s, t) + A_l^-(s, t) \tag{2.16}$$

where

$$A_l^\pm(s, t) = 8\pi \sum_{l=1}^\infty (2l + 1) A_l(t) \left(P_l(z_t) \pm P_l(-z_t) \right) \tag{2.17}$$

are known as even and odd signature amplitudes. In order to analytically continue from the region $t > 4m^2$, $s < 0$ to $t < 0$ and $s > 0$ it is assumed that the even and odd amplitudes are analytic in l throughout the $\mathrm{Re}(l) > 0$ plane with only isolated singularities. Hence

$$A^\pm(s, t) = 8\pi i \int_{\mathcal{C}} \mathrm{d}l (2l + 1) A^\pm(l, t) \frac{P_l(-z_t) \pm P_l(z_t)}{\sin(\pi l)}, \tag{2.18}$$

where $\mathcal{C}$ encircles all the l poles at $l = 0, 1, 2, \ldots$. Deforming the contour to a semi circle with infinite radius at $\mathrm{Re}(l) > -1/2$ gives

$$\begin{aligned} A^\pm(s, t) = &-16\pi^2 \sum_i \frac{(2\alpha_i^\pm(t) + 1)\beta_i^\pm(t)}{\sin\left(\pi\alpha_i^\pm(t)\right)} \left(P_{\alpha_i^\pm(t)}(-z_t) \pm P_{\alpha_i^\pm(t)}(z_t) \right) \\ &+ 8\pi i \int_{-\frac{1}{2}-i\infty}^{-\frac{1}{2}+i\infty} \mathrm{d}l \frac{(2l + 1) A^\pm(l, t) \left(P_l(-z_t) \pm P_l(z_t) \right)}{\sin(\pi l)} \end{aligned} \tag{2.19}$$

where the $\beta_i^{\pm}(t)$ are the residues and the $\alpha_i^{\pm}(t)$ are the corresponding locations in the complex l-plane. The procedure for this analytic continuation is quite subtle and discussed in appendix A of [19] and references therein. The second expression can be manipulated to become arbitrarily small (see again appendix A of [19] for details). Hence it will be dropped in the following. For large positive values of s, z_t is large negative and the asymptotic form of the Legendre polynomials can be used.

$$P_\alpha(z) \sim \begin{cases} \sqrt{\pi}\Gamma(\alpha+\frac{1}{2})/\Gamma(\alpha+1)(2z)^\alpha & \mathrm{Re}(\alpha) \geq \frac{1}{2} \\ \sqrt{\pi}\Gamma(-\alpha-\frac{1}{2})/\Gamma(-\alpha)(2z)^{(-\alpha-1)} & \mathrm{Re}(\alpha) \leq \frac{1}{2} \end{cases} \tag{2.20}$$

Using some simple Γ function algebra and some redefinitions of the residues $\beta_i^{\pm}(t)$

$$32\pi\Gamma(\alpha_i^{\pm}(t))\beta_i^{\pm} \to \beta_i^{\pm}(t)(2m^2 - \frac{1}{2}t)^{\alpha_i^{\pm}(t)}, \tag{2.21}$$

this gives the Regge representation of the amplitude, i.e. the high energy limit for small momentum transfer

$$A^{\pm}(s,t) \sim \sum_i \beta_i^{\pm}(t)\Gamma(-\alpha_i^{\pm}(t)) \underbrace{(1 \pm e^{-i\pi\alpha_i^{\pm}(t)})}_{=\xi_{\alpha_i}^{\pm}} (s/s_0)^{\alpha_i^{\pm}(t)}, \tag{2.22}$$

where $\xi_{\alpha_i}^{\pm}$ is called the signature factor, which corresponds to the phase δ_l of the amplitude discussed above.
For physical and even values of l, i.e. a non-negative even integer σ, the partial-wave amplitude near the pole behaves as

$$A_l(t) \sim A^+(t) \approx \frac{G(t)}{l - \alpha(t)}. \tag{2.23}$$

Expanding the amplitude around a linear Regge trajectory

$$\mathrm{Re}\,\alpha(t_0) = \sigma + \alpha'(t - t_0) \tag{2.24}$$

gives

$$A_\sigma \approx -\frac{G(t_0)/\alpha'}{t - t_0 + i\,\mathrm{Im}\,\alpha(t_0)/\alpha'}, \tag{2.25}$$

which is of the Breit-Wigner form for propagators with $\Gamma = \mathrm{Im}\,\alpha(m^2)/(\alpha' m)$

$$\Delta = \frac{1}{k^2 - m^2 + im\Gamma}. \tag{2.26}$$

Hence the Regge poles can be identified with particles whose masses lie on an approximately linear Regge trajectory.

2.1.4 Daughter trajectories

For unequal masses in the t-channel inital or final states one obtains an unphysical pole in the next-to-leading order term. This pole cancels for equal masses.

Consider for example the s-channel reaction $\pi^-\pi^+ \to K^-K^+$ with unequal masses in the t-channel initial or final states. The partial wave series is analogous to equation (2.10) with z_s replaced by z_t

$$A(s,t) = 16\pi \sum_{l=0}^{\infty} (2l+1) A_l(t) P_l(z_t), \tag{2.27}$$

with z_t given by

$$\begin{aligned} z_t =& 1 + \frac{s}{2|\mathbf{p}_t|^2} = 1 + \frac{st}{T(t)}, \\ 2T(t) =& t^2 - 2t(m_1^2 + m_2^2) + (m_1^2 + -m_2^2)^2. \end{aligned} \tag{2.28}$$

The redefinition of $\beta_0(t)$ for the Regge trajectory $\alpha_0(t)$ in equation (2.21) is now

$$32\pi\Gamma\left(\alpha_0(t) + \frac{3}{2}\right)\beta_0(t) \to \beta_0(t)(-T(t)/t)^{\alpha_0(t)}. \tag{2.29}$$

Using the asymptotic form of the Legendre polynomial $P_{\alpha_0(t)}(z_t)$ from equation (2.20) in (2.27) one additionally obtains a NLO term

$$s^{\alpha_0(t)} + \alpha_0(t) s^{\alpha_0(t)-1} T(t)/t \tag{2.30}$$

with a pole at $t = 0$. Cancelling this unphysical pole can be achieved by introducing a second reggeon $\alpha_1(t)$ with a simple pole in $\beta_1(t)$ at $t = 0$ and $\alpha_1(t) = \alpha_0(t) - 1$. However, this requires a third trajectory with $\alpha_2(t) = \alpha_0(t) - 2$ with a double pole on $\beta_2(t)$ at $t0 =$. In fact, one needs indefinitely many of these daughter trajectories to cancel all the singularities. These daughter trajectories are observed in meson spectroscopy when one considers the Chew-Frautschi plots of figure 2.1.

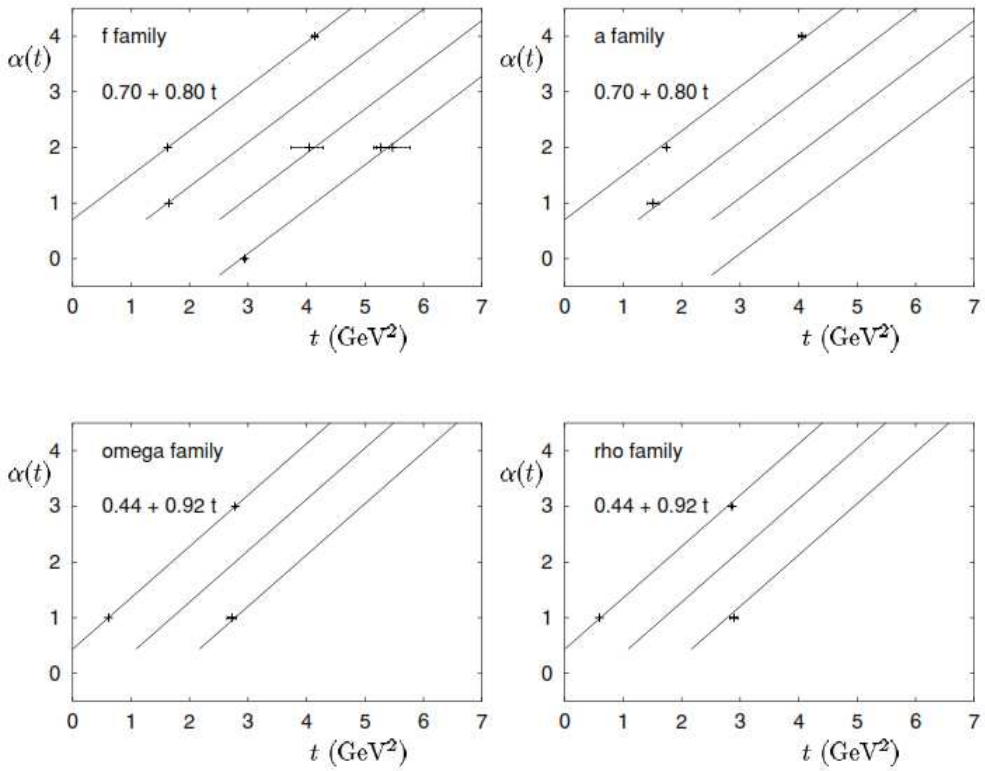

Figure 2.1: Families of daughter trajectories of some mesons where each parallel trajectories is one unit down in angular momentum. Plots from [19].

2.1.5 Spin

The previous discussion has neglected spin degrees of freedom, which will be treated in the following section. Again $1+2 \to 3+4$ scattering is considered in the CM frame. The helicity operator is given by

$$\frac{\mathbf{S}\cdot\mathbf{p}}{|\mathbf{p}|}\,|\lambda\rangle = \lambda\,|\lambda\rangle \tag{2.31}$$

where $|\lambda\rangle$ is a helicity eigenstate. Thus the differential cross section is obtained from

$$\frac{\mathrm{d}\sigma_\lambda}{\mathrm{d}\Omega} = \frac{|\mathbf{p_3}|}{64\pi^2|\mathbf{p_1}|s}|T_{\lambda_3,\lambda_4;\lambda_1\lambda_2}|^2 \tag{2.32}$$

with the transition operator now given by

$$T_{\lambda_3,\lambda_4;\lambda_1\lambda_2}(s,t) = \langle P_3,\lambda_3;P_4,\lambda_4|\,T\,|P_1,\lambda_1;P_2,\lambda_2\rangle\,. \tag{2.33}$$

Averaging over initial state helicities and summing over final states yields

$$\frac{\mathrm{d}\sigma}{\mathrm{d}\Omega} = \frac{1}{2s_1+1}\frac{1}{2s_2+1}\sum_{\lambda}\frac{\mathrm{d}\sigma_\lambda}{\mathrm{d}\Omega}. \tag{2.34}$$

Again, one can use a partial wave series as an ansatz for the amplitude, this time summing over the total angular momentum J

$$T_{\lambda_3,\lambda_4;\lambda_1\lambda_2}(s,t) = 16\pi\sum_{J\geq\mu}^{\infty}(2J+1)T^J_{\lambda_3,\lambda_4;\lambda_1\lambda_2}(s)d^J_{\lambda\lambda'}(\theta_s), \tag{2.35}$$

where $\lambda = \lambda_1 - \lambda_2$, $\lambda' = \lambda_3 - \lambda_4$, $\mu = \max(|\lambda|, |\lambda'|)$ and $d^J_{\lambda\lambda'}(\theta_s)$ is an element of the rotation matrix. Note that for the spinless case $d^J_{00} = P_J(\cos\theta_s)$ with $J = l$.
From parity and time-reversal invariance one finds

$$\begin{aligned} T_{-\lambda_3,-\lambda_4;-\lambda_1-\lambda_2} &= \eta(-1)^{s_3+s_4-s_1-s_2}T_{\lambda_3,\lambda_4;\lambda_1\lambda_2}, \\ T_{\lambda_1,\lambda_2;\lambda_3\lambda_4} &= T_{\lambda_3,\lambda_4;\lambda_1\lambda_2}, \end{aligned} \tag{2.36}$$

where $\eta = \eta_1\eta_2\eta_3\eta_4$ and the η_i are the intrinsic parities of the involved particles. Continuing the approach as in the previous section with Regge poles having definite parity, it is convenient to switch to t-channel helicity $T_{\tilde\lambda_2\tilde\lambda_4;\tilde\lambda_1\tilde\lambda_3}$ amplitudes with definite parity and their partial wave amplitudes given by

$$T^{J\pm}_{\tilde\lambda_2\tilde\lambda_4;\tilde\lambda_1\tilde\lambda_3}(t) = T_{\tilde\lambda_2\tilde\lambda_4;\tilde\lambda_1\tilde\lambda_3}(t) \pm \eta_1\eta_{\bar3}T_{\tilde\lambda_2\tilde\lambda_4;-\tilde\lambda_1-\tilde\lambda_3}(t). \tag{2.37}$$

The analysis of chapter 2.1.3 can now be repeated among similar lines.

2.2 The Tensor-Pomeron model

The Tensor-Pomeron model [22] was proposed by C. Ewertz, M. Maniatis and O. Nachtmann to provide a simple tool for calculating soft high energy scattering events such as CEP. In this model gauge invariant, effective Lagrangians are constructed using Regge theory and the Vector-Meson dominance model (VMD) to yield vertices and propagators which are compatible with the form of observed differential cross sections and which can be used in the standard QFT fashion. The coupling constants are then fitted to experimental data to be able to predict a large class of soft high energy processes. In this model, the Pomeron is constructed in a way to lie on a Regge trajectory starting at $J = 2$ and can be viewed as a coherent sum of even spin exchanges with vacuum quantum numbers (For a proof see appendix C).

What distinguishes the model from previous attempts to model pomeron exchange, is that it treats the pomeron predominantly as a gluonic object. For readability, only the necessary propagators and vertices are listed and some Lagrangians have been omitted. For a complete list see [22] as well as some extensions e.g. in [23].
The pomeron propagator is given by

$$\Delta_{\mu\nu\kappa\lambda}(s,t) = \frac{1}{4s}\left(g_{\mu\kappa}g_{\nu\lambda} + g_{\mu\lambda}g_{\nu\kappa} - \frac{1}{2}g_{\mu\nu}g_{\kappa\lambda}\right)(-is\alpha'_{\mathbb{P}})^{\alpha_{\mathbb{P}}(t)-1} \tag{2.38}$$

and the Regge trajectory is parametrized using

$$\begin{aligned}\alpha_{\mathbb{P}}(t) &= \alpha_{\mathbb{P}}(0) + \alpha'_{\mathbb{P}}t \\ \alpha_{\mathbb{P}}(0) &= 1.0808,\ \alpha'_{\mathbb{P}} = 0.25\text{GeV}^{-2}.\end{aligned} \tag{2.39}$$

The $\mathbb{P}pp$ vertex reads (see appendix C)

$$\Gamma_{\mu\nu}(p',p) = -3\beta_{\mathbb{P}NN}F_1\left((p'-p)^2\right)\left\{\frac{1}{2}[\gamma_\mu(p'+p)_\nu + \gamma_\nu(p'+p)_\mu] - \frac{1}{4}g_{\mu\nu}(\not{p}' + \not{p})\right\} \tag{2.40}$$

including a form factor

$$F_1(t) = \frac{1-(\mu_p/\mu_n)\frac{t}{4m_p^2}}{(1-\frac{t}{4m_p^2})(1-\frac{t}{m_D^2})}, \tag{2.41}$$

where $m_D^2 = 0.84\ \text{GeV}^2$ is the dipole mass, $\frac{\mu_p}{\mu_n} = 2.79$ is the fraction of the intrinsic magnetic moment of the proton and the neutron and $\beta_{\mathbb{P}NN} = 1.87\text{GeV}^{-1}$. The factor of 3 in $3\beta_{\mathbb{P}NN}$ accounts for the coupling to each valence quark and is pure convention.
The central exclusive production of η and η' mesons has already been discussed in [23], where the interaction Lagrangian is given by

$$\begin{aligned}\mathcal{L}'_{\mathbb{P}\mathbb{P}\tilde{M}} &= -\frac{2}{M_0}g'_{\mathbb{P}\mathbb{P}\tilde{M}}\partial_\rho\mathbb{P}_{\mu\nu}\partial_\sigma\mathbb{P}_{\kappa\lambda}g^{\mu\kappa}\epsilon^{\nu\lambda\rho\sigma}\tilde{\chi}, \\ \mathcal{L}''_{\mathbb{P}\mathbb{P}\tilde{M}} &= -\frac{g''_{\mathbb{P}\mathbb{P}\tilde{M}}}{M_0^3}\epsilon^{\mu_1\mu_2\nu_1\nu_2}\partial_{\mu_1}\tilde{\chi}\left(\partial_{\mu_3}\mathbb{P}_{\mu_4\nu_1} - \partial_{\mu_4}\mathbb{P}_{\mu_3\nu_1}\right)\overleftrightarrow{\partial}_{\mu_2} \\ &\quad\times(\partial^{\mu_3}\mathbb{P}^{\mu_4}_{\ \nu_2} - \partial^{\mu_4}\mathbb{P}^{\mu_3}_{\ \nu_2}),\end{aligned} \tag{2.42}$$

with $\overleftrightarrow{\partial}_\mu = \overrightarrow{\partial}_\mu - \overleftarrow{\partial}_\mu$ and $M_0 = 1\text{GeV}$. The effective pomeron field satisfies the following relations,

$$\begin{aligned} \mathbb{P}_{\kappa\lambda} &= \mathbb{P}_{\lambda\kappa}, \\ g^{\kappa\lambda}\mathbb{P}_{\kappa\lambda} &= 0. \end{aligned} \tag{2.43}$$

From this the vertex is readily obtained

$$\begin{aligned} \Gamma_{\mu\nu\kappa\lambda} =& \Gamma'_{\mu\nu\kappa\lambda} + \Gamma''_{\mu\nu\kappa\lambda}, \\ \Gamma'_{\mu\nu\kappa\lambda} =& \frac{g'_{\mathbb{PP}\tilde{M}}}{2M_0}(g_{\mu\kappa}\epsilon_{\nu\lambda\rho\sigma} + g_{\nu\kappa}\epsilon_{\mu\lambda\rho\sigma} + g_{\mu\lambda}\epsilon_{\nu\kappa\rho\sigma} + g_{\nu\lambda}\epsilon_{\mu\kappa\rho\sigma} \\ & \times (q_1 - q_2)^\rho (q_1 + q_2)^\rho F_{\mathbb{PP}\tilde{M}}(q_1^2, q_2^2), \\ \Gamma''_{\mu\nu\kappa\lambda} =& \frac{g''_{\mathbb{PP}\tilde{M}}}{M_0^3}\epsilon_{\nu\lambda\rho\sigma}[k_{1\kappa}k_{2\mu} - (q_1q_2)g_{\mu\kappa}] \\ & + \epsilon_{\mu\lambda\rho\sigma}[k_{1\kappa}k_{2\nu} - (q_1q_2)g_{\nu\kappa}] + \epsilon_{\nu\kappa\rho\sigma}[k_{1\lambda}k_{2\mu} - (q_1q_2)g_{\mu\lambda}] \\ & + \epsilon_{\mu\kappa\rho\sigma}[k_{1\lambda}k_{2\nu} - (q_1q_2)g_{\nu\lambda}] \\ & \times (q_1 - q_2)^\rho (q_1 + q_2)^\sigma F_{\mathbb{PP}\tilde{M}}(q_1^2, q_2^2). \end{aligned} \tag{2.44}$$

In constructing these vertices in a covariant fashion, it is crucial to think of the possible combinations of J and P that mesons getting produced in pomeron fusion can have. Constructing the pomeron states using spherical harmonics and Clebsh-Gordan coefficients one finds that parity transformations act like

$$\hat{P}\,|S, S_z; l, l_z\rangle = (-1)^l\,|S, S_z; l, l_z\rangle \tag{2.45}$$

and the two-pomeron state is given by

$$|l, S; J, J_z\rangle = \sum_{S_z, l_z} \langle S, S_z; l, l_z | J, J_Z\rangle\,|S, S_z; l, l_z\rangle\,. \tag{2.46}$$

Thinking of pomeron fusion in CEP as containing a subprocess where two pomerons decay into one meson with total spin $|l-S| \leq J \leq l+S$ and parity $P = (-1)^l$, it is easy to construct possible final meson states with quantum numbers given in table 2.1. Note that Bose symmetry of the pomeron requires that $|S, S_z; l, l_z\rangle = 0$ for $l - S$ odd.

l	S	J	P
0	0	0	+
	2	2	
1	1	0,1,2	−
	3	2,3,4	
2	0	2	+
	2	0,1,2,3,4	
3	1	2,3,4	−
	3	0,1,...,6	
4	0	4	+
	2	2,3,4,5,6	
	4	0,1,...,8	

Table 2.1: Possible quantum numbers J^P for mesons produced in pomeron fusion.

So for pseudoscalar meson production the two lowest lying (l,S) components are (1,1) and (3,3) corresponding to $g'_{\mathbb{PP}\tilde{M}}$ and $g''_{\mathbb{PP}\tilde{M}}$, respectively. For (axial) vector meson production, which is currently being worked out in the Tensor-Pomeron model by Nachtmann et al., the two lowest lying components are (2,2) and (4,4).

The numerical values for the couplings are obtained from fits to experimental data and are given in table 2.2.

	$g'_{\mathbb{PP}\tilde{M}}$	$g''_{\mathbb{PP}\tilde{M}}$
η	2	2.25
η'	2.61	1.5

Table 2.2: Fitted coupling constants for (l,S)=$\{(1,1),(3,3)\}$ to WA102 data from [23].

Note that for η' meson production due to the high glue component of the mass eigenstate (see appendix B.3 for details) it is sufficient to only consider pomeron fusion, whereas for the lighter η particle one also should take reggeon exchange into account. This has been discussed in [23] as well as [24].

In the framework of the Tensor-Pomeron model the $(2,2)$ and $(4,4)$ couplings, $g'_{\mathbb{PP}f_1}$ and $g''_{\mathbb{PP}f_1}$, of the f_1 meson to two pomerons are given by the following interaction Lagrangians [25]

$$\begin{aligned}\mathcal{L}'_{\mathbb{PP}f_1} =& \frac{1}{32M_0^2} g_{\mathbb{PP}f_1} (\mathbb{P}_{\kappa\lambda} (\overleftrightarrow{\partial}_\mu \overleftrightarrow{\partial}_\nu \mathbb{P}_{\rho\sigma}) (\partial_\alpha U_\beta - \partial_\beta U_\alpha)) \\ & \times \Gamma^{(8)\kappa\lambda\rho\sigma\mu\nu\alpha\beta} F'^{\mathbb{PP}f_1}(q_1^2, q_2^2),\end{aligned} \tag{2.47}$$

$$\begin{aligned}\mathcal{L}''_{\mathbb{PP}f_1} =& \frac{g''_{\mathbb{PP}f_1}}{24 \cdot 32M_0^4} \mathbb{P}_{\kappa\lambda} \left(\overleftrightarrow{\partial}_{\mu_1} \overleftrightarrow{\partial}_{\mu_2} \overleftrightarrow{\partial}_{\mu_3} \overleftrightarrow{\partial}_{\mu_4}\right) \mathbb{P}_{\rho\sigma} \times \\ & (\partial_\alpha U_\beta - \partial_\beta U_\alpha)\, \Gamma^{(10)\kappa\lambda,\rho\sigma,\mu_1\mu_2\mu_3\mu_4,\alpha\beta} F''^{\mathbb{PP}f_1}(q_1^2, q_2^2),\end{aligned} \tag{2.48}$$

where $M_0 = 1\text{GeV}$ and an auxiliary rank 8 tensor

$$\begin{aligned}\Gamma^{(8)\kappa\lambda\rho\sigma\mu\nu\alpha\beta} =& g^{\kappa\rho} g^{\lambda\mu} \epsilon^{\sigma\nu\alpha\beta} + g^{\kappa\sigma} g^{\lambda\mu} \epsilon^{\rho\nu\alpha\beta} - g^{\lambda\mu} g^{\rho\sigma} \epsilon^{\kappa\nu\alpha\beta} \\ & + g^{\kappa\rho} g^{\lambda\nu} \epsilon^{\sigma\mu\alpha\beta} + g^{\kappa\sigma} g^{\lambda\nu} \epsilon^{\rho\mu\alpha\beta} + g^{\kappa\mu} g^{\lambda\rho} \epsilon^{\sigma\nu\alpha\beta} \\ & + g^{\kappa\nu} g^{\lambda\rho} \epsilon^{\sigma\mu\alpha\beta} + g^{\kappa\mu} g^{\lambda\sigma} \epsilon^{\rho\nu\alpha\beta} + g^{\kappa\nu} g^{\lambda\sigma} \epsilon^{\rho\mu\alpha\beta} \\ & - g^{\kappa\lambda} g^{\mu\rho} \epsilon^{\sigma\nu\alpha\beta} + g^{\kappa\sigma} g^{\mu\rho} \epsilon^{\lambda\nu\alpha\beta} + g^{\lambda\sigma} g^{\mu\rho} \epsilon^{\kappa\nu\alpha\beta} \\ & - g^{\kappa\lambda} g^{\mu\sigma} \epsilon^{\rho\nu\alpha\beta} + g^{\kappa\rho} g^{\mu\sigma} \epsilon^{\lambda\nu\alpha\beta} + g^{\lambda\rho} g^{\mu\sigma} \epsilon^{\kappa\nu\alpha\beta} \\ & - g^{\kappa\lambda} g^{\nu\rho} \epsilon^{\sigma\mu\alpha\beta} + g^{\kappa\sigma} g^{\nu\rho} \epsilon^{\lambda\mu\alpha\beta} + g^{\lambda\sigma} g^{\nu\rho} \epsilon^{\kappa\mu\alpha\beta} \\ & - g^{\kappa\lambda} g^{\nu\sigma} \epsilon^{\rho\mu\alpha\beta} + g^{\kappa\rho} g^{\nu\sigma} \epsilon^{\lambda\mu\alpha\beta} + g^{\lambda\rho} g^{\nu\sigma} \epsilon^{\kappa\mu\alpha\beta} \\ & - g^{\kappa\mu} g^{\rho\sigma} \epsilon^{\lambda\nu\alpha\beta} - g^{\kappa\nu} g^{\rho\sigma} \epsilon^{\lambda\mu\alpha\beta} - g^{\lambda\nu} g^{\rho\sigma} \epsilon^{\kappa\mu\alpha\beta},\end{aligned} \tag{2.49}$$

rank 10 tensor

$$\begin{aligned}\Gamma^{(10)}_{\kappa\lambda,\rho\sigma,\mu_1\mu_2\mu_3\mu_4,\alpha\beta} =& \{[(g_{\kappa\mu_1} g_{\lambda\mu_2} - \frac{1}{4} g_{\kappa\lambda} g_{\mu_1\mu_2} \\ & \times (g_{\rho\mu_3} \epsilon_{\sigma\mu_4\alpha\beta} - \frac{1}{4} g_{\rho\sigma} \epsilon_{\mu_3\mu_4\alpha\beta}) \\ & + (\kappa \leftrightarrow \lambda) + (\rho \leftrightarrow \sigma) + (\kappa \leftrightarrow \lambda, \rho \leftrightarrow \sigma)] \\ & + (\kappa, \lambda) \leftrightarrow (\rho, \sigma)\} \\ & + \text{all permutations of } (\mu_1, \mu_2, \mu_3, \mu_4),\end{aligned} \tag{2.50}$$

and form factors $F'^{\mathbb{PP}f_1}(q_1^2, q_2^2)$,$F''^{\mathbb{PP}f_1}(q_1^2, q_2^2)$ have been introduced. This yields the vertices

$$\begin{aligned}i\Gamma^{\mathbb{PP}f_1\prime}_{\kappa\lambda\rho\sigma\alpha}(q_1, q_2) =& -\frac{g'_{\mathbb{PP}f_1}}{8M_0^2} (q_1 - q_2)^\mu (q_1 - q_2)^\nu (q_1 + q_2)^\beta \Gamma^{(8)}_{\kappa\lambda\rho\sigma\mu\nu\alpha\beta} F'^{\mathbb{PP}f_1}(q_1^2, q_2^2) \\ =& i\frac{g'_{\mathbb{PP}f_1}}{M_0^2} (q_1 - q_2)^\mu (q_1 - q_2)^\nu (q_1 + q_2)^\beta \\ & \times (g_{\kappa\rho} g_{\mu\sigma} \epsilon_{\lambda\nu\alpha\beta} + g_{\kappa\rho} g_{\mu\lambda} \epsilon_{\sigma\nu\alpha\beta}) F'^{\mathbb{PP}f_1}(q_1^2, q_2^2)\end{aligned} \tag{2.51}$$

and

$$i\Gamma^{\mathbb{PP}f_1\prime\prime}_{\kappa\lambda\rho\sigma\alpha}(q_1,q_2) = \frac{g''_{\mathbb{PP}f_1}}{8\cdot 24M0^4} q_{12}^{\mu_1} q_{12}^{\mu_2} q_{12}^{\mu_3} q_{12}^{\mu_4} (q_1+q_2)^{\beta} \Gamma^{(10)}_{\kappa\lambda,\rho\sigma,\mu_1\mu_2\mu_3\mu_4,\alpha\beta} F''^{\mathbb{PP}f_1}(q_1^2,q_2^2)$$
$$\frac{g''_{\mathbb{PP}f_1}}{2M_0^4} q_{12,\kappa} q_{12,\rho} q_{12}^{\mu} (q_1+q_2)^{\beta} (q_{12,\lambda}\epsilon_{\sigma\alpha\mu\beta} + q_{12,\sigma}\epsilon_{\lambda\alpha\mu\beta}) F''^{\mathbb{PP}f_1}(q_1^2,q_2^2) \tag{2.52}$$

where $q_{12} = q_1 - q_2$.

2.3 The Witten-Sakai-Sugimoto model

A full treatment of the Witten-Sakai-Sugimoto model is beyond the scope of this work and the following section, as well as appendix D, should only capture the key concepts of the underlying theory. For a review and some recent results see for example [26].

Already in 1974, through his studies of planar diagrams [27] in large-N_c theories with fixed t'Hooft coupling, $\lambda = g^2 N_c$, Gerard t'Hooft speculated about large-N_c theories being essentially a limit of string theory. The AdS/CFT correspondence (see [28] or [29] for reviews), a realisation of this idea formulated by Juan Maldacena in 1997 [30], can be used to relate strongly coupled large N_c supersymmetric Yang-Mills (SYM) theories to supergravity, which is essentially a low energy limit of string theory, in anti-de Sitter space. This correspondence can be generalized to nonconformal supersymmetric theories by either a manual breaking of conformal invariance (Bottom-up approach) or by a first-principles construction from superstring theory with nonconformal D-Branes (Top-down). The latter is used in the Witten model, where Type-IIA string theory with a large number of N_c D4 branes is used to create a dual to 4+1 dimensional SYM theory. Supersymmetry is then broken by a certain compactification to get to a 3+1 dimensional space-time and the resulting model is dual to pure-glue YM theory below the compactification scale [4]. From this action the glueball spectrum can be calculated.

In [3] Sakai and Sugimoto extended the model by adding flavour branes to include fermions. This results in an effective action including hadrons as well as glueballs.

The Witten background which will generate confinement in the dual theory is given by

$$\begin{aligned} \mathrm{d}s^2 &= G_{MN}\mathrm{d}x^M\mathrm{d}x^N \\ &= \left(\frac{u}{R}\right)^{\frac{3}{2}}\left[\eta_{\mu\nu}\mathrm{d}x^\mu\mathrm{d}x^\nu + f(u)\mathrm{d}x_4^2\right] + \left(\frac{R}{u}\right)^{\frac{3}{2}}\left[\frac{\mathrm{d}u^2}{f(u)} + u^2\mathrm{d}\Omega_4^2\right] \\ e^\phi &= g_s\left(\frac{u}{R}\right)^{3/4}, \;\; F_4 = \mathrm{d}C_3 = \frac{2\pi N_c}{V_4}\epsilon_4, \\ f(u) &= 1 - \frac{u_{KK}^3}{u^3}, \quad M_{KK} = \frac{3}{2}\frac{u_{KK}^{1/2}}{R^{3/2}}, \end{aligned} \tag{2.53}$$

including a dilaton e^ϕ, Ramond-Ramond 3-form C_3 with ϵ_4 being the volume form and V_4 the volume of a unit S_4 and radial coordinate $u \geq u_{KK}$, and the gravity action is

$$S_{grav} = \frac{1}{2\kappa_{10}^2}\int \mathrm{d}^{10}x\sqrt{-g}\left[e^{-2\phi}\left(R + 4(\nabla\phi)^2 - \frac{(2\pi)^4 l_s^2}{2\cdot 4!}F_4^2\right)\right]. \tag{2.54}$$

The spectrum of the spin 2 glueballs, which are dual to modes of the background graviton field h_{MN}, is obtained from the Einstein-Hilbert action (2.54) expanded in metric fluctuations $g_{MN} = G_{MN} - h_{MN}$ around the Witten background (2.53) which gives the equations of motion for the graviton h_{ij}[1] [31]

$$-\frac{1}{2}\left(\frac{9f}{2} + 3u\partial_u f\right)h_{ij} + (f + u\partial_u f)u\partial_u h_{ij} + fu^2\partial_u^2 h_{ij} = -\frac{q^2R^3}{u}h_{ij} \tag{2.55}$$

where q^2 is the 4-momentum squared. Choosing boundary conditions such that the solution is smooth at $u = u_{KK}$ and normalizable as $u \to \infty$ and making a mode ansatz

$$h_{ij}(x,u) = \sum_{n=1}^{\infty} h_{ij}^{(n)}(x)\left(\frac{u}{R}\right)^{3/2}T_n(u) \tag{2.56}$$

with resonances $h_{ij}^{(n)}$ of mass m_n^2 and wave functions $T_n(u)$ that satisfy

$$\partial_u(u^4 f\partial_u T_n) = -m_n^2 R^3 u T_n. \tag{2.57}$$

The lightest resonance has mass $m_1^2 = 1.57M_{KK}^2$ and corresponds to the first state on the pomeron trajectory whilst higher resonances correspond to daughter trajectories. The ansatz (2.56) can now be used in the gravity action (2.54) which gives

[1] The gauge chosen is $h_{0\mu} = 0$

$$\begin{aligned}\mathcal{L}_{grav} \supset & \frac{N_c^3 M_{kk}^2 g_{YM}^2}{3^5\pi^2}\int_1^\infty \frac{u}{u_{KK}} T_1^2 \mathrm{d}\left(\frac{u}{u_{kk}}\right) \\ & \times \int \mathrm{d}^4x \eta^{\mu\nu}\eta^{\beta\delta}\eta^{\alpha\gamma}\left[\partial_\alpha h_{\delta\nu}\partial_\mu h_{\beta\gamma} - \frac{1}{2}\partial_\alpha h_{\delta\nu}\partial_\gamma h_{\beta\mu}\right] + \cdots\end{aligned} \tag{2.58}$$

Requiring a canonical normalization of the kinetic terms
to obtain a canonical normalization of the kinetic terms one requires

$$\frac{2N_c^3 M_{kk}^2 g_{YM}^2}{3^5\pi^2}\int_1^\infty \frac{u}{u_{KK}} T_1^2 \mathrm{d}\left(\frac{u}{u_{KK}}\right) = 1. \tag{2.59}$$

The propagator for a massive spin-2 field is given as in [32] by

$$\begin{aligned}\Delta_{\mu\rho\nu\sigma}(k) =& \frac{-id_{\mu\rho\nu\sigma}}{k^2 - m_g^2} \\ d_{\mu\rho\nu\sigma} =& \frac{1}{2}\left(\eta_{\mu\nu}\eta_{\rho\sigma} + \eta_{\mu\sigma}\eta_{\rho\nu}\right) \\ & - \frac{1}{2m_g^2}(k_\mu k_\sigma \eta_{\rho\nu} + k_\mu k_\nu \eta_{\rho\sigma} + k_\rho k_\sigma \eta_{\mu\nu} + k_\rho k_\nu \eta_{\mu\sigma}) \\ & + \frac{1}{24}\left[\left(\frac{k^2}{m_g^2}\right)^2 - 3\left(\frac{k^2}{m_g^2}\right) - 6\right]\eta_{\mu\rho}\eta_{\nu\sigma} \\ & - \frac{k^2 - 3m_g^2}{6m_g^4}(k_\mu k_\rho \eta_{\nu\sigma} + k_\nu k_\sigma \eta_{\mu\rho}) + \frac{k_\mu k_\rho k_\nu k_\sigma}{3m_g^4},\end{aligned} \tag{2.60}$$

where only the first line will end up contributing when contracted with the vertices for the central exclusive production of pseudoscalar and axial vector mesons. Assuming that the glueball primarily couples to the stress-energy tensor of the protons, the proton-proton-glueball vertex can be written as [33]

$$\begin{aligned}\Gamma^{\mu\rho}(p', p) =& \lambda_P\left[\frac{A(t)}{2}(\gamma^\mu P^\rho + \gamma^\rho P^\mu)\right. \\ & + \frac{B(t)}{8m_p}(P^\mu[\gamma^\rho, \gamma^\nu] + P^\rho[\gamma^\mu, \gamma^\nu])k_\nu \\ & \left. - \frac{C(t)}{m_p}(\eta^{\mu\rho}t + k^\mu k^\rho)\right]\end{aligned} \tag{2.61}$$

where

$$\begin{aligned} P &= \frac{p' + p}{2}, \\ k &= p' - p, \end{aligned} \tag{2.62}$$

and

$$A(t) = \frac{1}{(1 - \frac{t}{M_D^2})^2}, \tag{2.63}$$

a form factor with $M_D = 1.17$ GeV from Sakai-Sugimoto model predictions. Note that the term proportional to $C(t)$ will vanish when contracted with the propagators and the pseudoscalar or axial vector vertex, respectively. In Ref.[34] it was shown that $B(t)$ can be neglected in central exclusive production when the Regge limit is considered, hence it will be dropped in the following calculations.

Following the procedure of [33] by reggeizing the scattering amplitude of four closed strings, the reggeized propagator is given by

$$\frac{1}{t - m_g^2} \to \frac{\alpha_c' \Gamma[-\chi]^2 \Gamma[1 - \frac{\alpha_c(t)}{2}]}{2\Gamma[\frac{\alpha_c(t)}{2} - 1 - \chi]} \left(-\frac{i\alpha_c' s}{s} \right)^{\alpha_c(t)-2}, \tag{2.64}$$

with

$$\begin{aligned} \alpha_c(t) &= 2 - \alpha_c' m_g^2 + \alpha_c' t, \\ \chi &= \frac{\alpha_c'}{2}(4m_p^2 - 3m_g^2). \end{aligned} \tag{2.65}$$

The interaction Lagrangian resulting from the Chern-Simons action, which gives the couplings to the mesons of interest, is given by [35]

$$\begin{aligned} \mathcal{L}_{CS} \supset\ & \kappa_a \epsilon^{\mu\nu\rho\sigma} \eta_0 \partial_\nu h_{\alpha\mu} \partial_\sigma h_\rho^\alpha + \kappa_b \epsilon^{\mu\nu\rho\sigma} \eta_0 \partial_\nu \partial^\alpha h_{\mu\beta} \left(\partial_\sigma \partial^\beta h_{\alpha\rho} - \partial_\sigma \partial_\alpha h_\rho^\beta \right) \\ & + \kappa_c a_\alpha^0 \epsilon^{\alpha\beta\gamma\delta} h_\beta^\mu \partial_\delta h_{\gamma\mu} + \kappa_d a_\alpha^0 \epsilon^{\alpha\beta\gamma\delta} \partial_\nu h_\beta^\mu \left(\partial_\delta \partial_\mu h_\gamma^\nu - \partial_\delta \partial_\nu h_\gamma^\mu \right), \end{aligned} \tag{2.66}$$

where

$$\begin{aligned}\kappa_a &= -\frac{33.3060\sqrt{N_f}}{M_{KK}\sqrt{N_c^3\lambda^3}} \\ &= -0.172503\text{GeV}^{-1}, \\ \kappa_b &= \frac{64.7935\sqrt{N_f}}{M_{KK}^3\sqrt{N_c^3\lambda^3}} \\ &= 0.372643\text{GeV}^{-3}\end{aligned} \tag{2.67}$$

are the pseudoscalar and

$$\begin{aligned}\kappa_c &= \frac{2522.75\sqrt{N_f}}{\sqrt{N_c^3\lambda^3}} \\ &= 12.3998, \\ \kappa_d &= -\frac{708.021\sqrt{N_f}}{M_{KK}^2\sqrt{N_c^3\lambda^3}} \\ &= -3.86415\text{GeV}^{-2}\end{aligned} \tag{2.68}$$

are the axial vector couplings, respectively.

The resulting tree level vertices are given by

$$\begin{aligned}\mathrm{V}_{\mathbb{PP}\eta}^{\mu_1\nu_1\mu_2\nu_2} &= -2\epsilon^{\mu_1\mu_2\alpha\beta}q_1^\alpha q_2^\beta\left(g^{\nu_1\nu_2}(\kappa_a+\kappa_b(q_1q_2))-\kappa_b q_1^{\nu_2}q_2^{\nu_1}\right) \\ \mathrm{V}_{\mathbb{PP}f}^{\mu_1\mu_2\nu_2\mu_3\nu_3} &= -2g_{\alpha\beta}\epsilon^{\mu_1\mu_2\mu_3\alpha}(q_1-q_2)^\beta\left(g^{\nu_2\nu_3}(\kappa_d(q_1q_2)+\kappa_c)-\kappa_d q_1^{\nu_3}q_2^{\nu_2}\right).\end{aligned} \tag{2.69}$$

Note that κ_a roughly corresponds to $g'_{\mathbb{PP}\tilde{M}}$ in the Tensor-Pomeron model which is the $(l,S)=(1,1)$ coupling to mesons with quantum number $J^P=0^-$. Similarly, κ_b roughly corresponds to $g''_{\mathbb{PP}\tilde{M}}$ representing the $(l,S)=(3,3)$ coupling to mesons with $J^P=0^-$. However, $g'_{\mathbb{PP}f_1}$, does not correspond to κ_d as one would suggest from a simple counting of derivatives. A closer examination of the index structure of both vertices reveals that in the Tensor-Pomeron model, the pomeron only couples to the field strength of the f_1 meson, similarly as in the case of the magnetic moment. Whereas in the holographic approach one obtains a minimal coupling of the mesons. However, they do agree on-shell as was shown by Nachtmann [25] with the identification

$$\frac{g'_{\mathbb{PP}f_1}}{M_0^2}k^2 = -\kappa_c. \tag{2.70}$$

So for an on-shell f_1 meson $k^2 = m_{f_1}^2$ whereas a broad resonance rather introduces an additional form factor

$$F(k^2) = \frac{k^2}{m_{f_1}^2}. \tag{2.71}$$

In section 3.3 the difference of these couplings will be studied further and it will be shown, that there is a leading order contribution from taking the Regge limit of the κ_c term that does not arise for the $g'_{\mathbb{PP}f_1}$ coupling.

A similiar identification leads to a one-to-one correspondence between the κ_d term and the $g''_{\mathbb{PP}f_1}$ term [35].

2.4 Further possible couplings

Following the principles of gauge invariance and renormalisation, one can find further possible interaction terms that couple an axial vector field $\mathcal{A}$ to spin-2 fields h with up to three derivatives [35]

$$\mathcal{L}^1_{int} = \mathcal{A}_\mu h_{\alpha\sigma}\epsilon^{\mu\nu\rho\sigma}\partial_\nu h^\alpha_\rho \tag{2.72a}$$
$$\mathcal{L}^2_{int} = \mathcal{A}_\mu \epsilon^{\mu\nu\rho\sigma}\partial_\nu h^\beta_\alpha \partial_\rho \partial^\alpha h_{\beta\sigma} \tag{2.72b}$$
$$\mathcal{L}^3_{int} = \mathcal{A}_\mu \epsilon^{\mu\nu\rho\sigma}\partial^\alpha \partial_\alpha h_{\beta\sigma}\partial_\nu h^\beta_\rho \tag{2.72c}$$
$$\mathcal{L}^4_{int} = \mathcal{A}_\mu \epsilon^{\mu\nu\rho\sigma}\partial_\alpha h_{\beta\sigma}\partial_\nu \partial^\alpha h^\beta_\rho \tag{2.72d}$$
$$\mathcal{L}^5_{int} = \mathcal{A}_\mu h_{\beta\sigma}\epsilon^{\mu\nu\rho\sigma}\partial_\nu \partial^\alpha h^\beta_\rho \tag{2.72e}$$
$$\mathcal{L}^6_{int} = \mathcal{A}_\mu \epsilon^{\mu\nu\rho\sigma}\partial^\beta h_{\alpha\sigma}\partial_\nu \partial^\alpha h_{\beta\rho} \tag{2.72f}$$
$$\mathcal{L}^7_{int} = \mathcal{A}^\alpha \epsilon^{\mu\nu\rho\sigma}\partial_\mu \partial_\alpha h^\beta_\rho \partial_\nu h_{\beta\rho} \tag{2.72g}$$
$$\mathcal{L}^8_{int} = \mathcal{A}^\alpha \epsilon^{\mu\nu\rho\sigma}\partial_\mu h_{\beta\rho}\partial_\nu \partial^\beta h_{\alpha\sigma} \tag{2.72h}$$

It can be shown that (2.72a)-(2.72f) are equal to the κ_c, κ_d or $g'_{\mathbb{PP}f_1}$ (on-shell), $g''_{\mathbb{PP}f_1}$ terms, respectively. The seventh and eigth term however do not emerge naturally in the Sakai-Sugimoto model and will be further studied in section 3.4. The resulting vertices for these interaction Lagrangians are given at tree level by

$$\begin{aligned} V_7^{\mu_1\mu_2\nu_2\mu_3\nu_3} &= (q_1+q_2)^{\mu_1} q_{1\alpha} q_{2\beta} g^{\mu_2\mu_3}\epsilon^{\nu_2\nu_3\alpha\beta}, \\ V_8^{\mu_1\mu_2\nu_2\mu_3\nu_3} &= \epsilon^{\nu_2\nu_3\alpha\beta} q_{1\alpha} q_{2\beta}(q_1^{\mu_3} g^{\mu_1\mu_2} + q_2^{\mu_2} g^{\mu_1\mu_3}). \end{aligned} \tag{2.73}$$

2.5 Non-linear Regge trajectories

Linear behaviour of real Regge trajectories for baryons and mesons is a good approximation to experimental observations [20]. This produces however infinitely narrow resonances. One approach to cure this problem is to consider complex non-linear trajectories as was done in [36]. As ansatz they considered

$$\alpha(t) = \frac{1 + \delta + \alpha_1 t}{1 + \alpha_2 \sqrt{t_0 - t} - \sqrt{t_0}}, \tag{2.74}$$

where $t_0 = 4m_\pi^2$ is the threshold. The parameters where then fitted to data from the TOTEM experiment at LHC and are summarized in table A.4.

Chapter 3

Central exclusive production of pseudoscalar and axial vector mesons

In the following the central exclusive production of pseudoscalar and axial vector mesons is considered. The high-energy-small-angle or Regge limit is used where the transverse momenta of the outgoing protons, which are initially zero, are considered to be small. This corresponds to the class of experiments that were carried out from the WA102 collaboration. The invariant variables for this process are discussed and the phase space is parametrized in this limit. Finally the differential cross sections for the production of η' and f_1 mesons are calculated and fitted to experimental data.

3.1 Regge limit and phase space

The Mandelstam variables are chosen in the standard convention (see e.g. [37] for further relations) and a mostly minus convention is used for the metric. The momenta $p_a,\ p_b,\ p_1$ and p_3 correspond to the ingoing and outgoing protons, whilst p_2 is the momentum of the outgoing meson (see figure 3.1). Hence

$$\begin{aligned} &p_a^2 = p_b^2 = p_1^2 = p_3^2 = m_p^2,\ p_2^2 = m_2^2, \\ &q_1 = (p_a - p_1),\ q_2 = (p_b - p_3). \end{aligned} \tag{3.1}$$

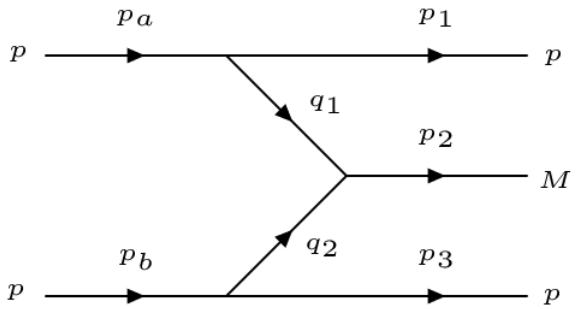

Figure 3.1: Kinematics for the central exclusive production of a meson M in peripheral pp collisions.

This gives the standard representation of the Mandelstam variables, which will be used throughout the whole calculation

$$\begin{aligned} s &= s_{ab} = (p_a + p_b)^2 = (p_1 + p_2 + p_3)^2, \\ s_1 &= s_{12} = (p_1 + p_2)^2 = (p_a + p_b - p_3)^2, \\ s_2 &= s_{23} = (p_2 + p_3)^2 = (p_a + p_b - p_1)^2, \\ t_1 &= t_{a1} = (p_a - p_1)^2 = (p_2 + p_3 - p_b)^2, \\ t_2 &= t_{b3} = (p_b - p_3)^2 = (p_1 + p_2 - p_a)^2. \end{aligned} \tag{3.2}$$

The total cross section is given by

$$\sigma = \frac{1}{2E_a 2E_b |v_a - v_b|} \int \mathrm{dLIPS}_3 |\overline{\mathcal{A}}|^2, \tag{3.3}$$

where

$$\mathrm{dLIPS}_3 = \left(\prod_{i=3}^{5} \int \frac{\mathrm{d}^3 p_i}{(2\pi)^3 2E_i} \right) (2\pi)^4 \delta^4 (p_a + p_b - p_1 - p_2 - p_3) \tag{3.4}$$

is the Lorentz invariant phase space measure and $|\overline{\mathcal{A}}|^2$ is the spin averaged amplitude squared.

Using equation (3.2) and the on shell conditions in the CM frame and

$$
\begin{aligned}
&v_a = \frac{p_a^z}{E_a},\ v_b = \frac{p_b^z}{E_b},\\
&s = 2m_p^2 + 2(p_a p_b),\\
&E_a = E_b = \frac{\sqrt{s}}{2},\\
&E_{1,3} = \sqrt{\mathbf{p}_{1,3}^2 + m_p^2},\\
&E_2 = \sqrt{(\mathbf{p_1} + \mathbf{p_3})^2 + m_2^2},\\
&|v_a - v_b| = \frac{2}{\sqrt{s}}\sqrt{(p_a p_b) - m_p^2},
\end{aligned}
\tag{3.5}
$$

to integrate out the $\mathbf{p}_2$ dependence, one finds

$$
\sigma = \frac{2\pi}{2^6\sqrt{(p_a p_b)^2 - m_p^4}} \int \frac{|\overline{\mathcal{A}}|^2 \delta(2E_a - E_1 - E_2 - E_3)}{E_1 E_2 E_3} \frac{\mathrm{d}^3\mathbf{p_1}}{(2\pi)^3} \frac{\mathrm{d}^3\mathbf{p_3}}{(2\pi)^3}. \tag{3.6}
$$

The angular integrations can be parametrized in the following way [1]

$$
\begin{aligned}
&p_1 = \left(E_1, \mathbf{p_{1\perp}}, p_{1z}\right)^T \ \ p_3 = \left(E_3, \mathbf{p_{3\perp}}, p_{3z}\right)^T\\
&\mathbf{p_{1,3_\perp}} = p_{1,3_\perp}\left(\cos\theta_{1,3}, \sin\theta_{1,3}\right)^T\\
&\theta_1 = \phi,\ \theta_{13} = \theta_3 - \theta_1,\ p_{1z} = x_1 p,\ p_{3z} = x_3 p\\
&p_{1z} + p_{3z} = p x_F,\ p_{1z} - p_{3z} = p_{-z},
\end{aligned}
\tag{3.7}
$$

with the corresponding differentials

$$
\begin{aligned}
&\mathrm{d}^3\mathbf{p_1}\mathrm{d}^3\mathbf{p_3} = \frac{1}{4}\mathrm{d}(p_{1\perp})^2\mathrm{d}(p_{3\perp})^2\mathrm{d}\theta_1\mathrm{d}\theta_3\mathrm{d}p_{1z}\mathrm{d}p_{3z}\\
&\mathrm{d}\theta_1\mathrm{d}\theta_3 = \mathrm{d}\phi\mathrm{d}\theta_{13}\\
&\mathrm{d}p_{1z}\mathrm{d}p_{3z} = \frac{p}{2}\mathrm{d}x_F\mathrm{d}p_{-z}.
\end{aligned}
\tag{3.8}
$$

Plugging everything in and integrating out the p_{-z} and ϕ dependence gives

$$
\sigma = \frac{p}{2^8(2\pi)^4\sqrt{(p_a p_b)^3 - m_p^4}} \int \frac{|\overline{\mathcal{A}}|^2}{E_2|p_{3z}E_1 - p_{1z}E_3|}\mathrm{d}\theta_{13}\mathrm{d}x_F\mathrm{d}(p_{1\perp})^2\mathrm{d}(p_{3\perp})^2. \tag{3.9}
$$

[1] See e.g [33] for details

To apply the Regge limit, it is useful to express p, p_{1z}, p_{3z} in terms of Mandelstam variables. One finds

$$\begin{aligned} p &= \frac{1}{2}\sqrt{s-4m_p^2}, \\ p_{1z} &= \frac{s-s_2+2t_1-3m_p^2}{2\sqrt{s-4m_p^2}}, \\ p_{3z} &= \frac{-s+s_1-2t_2-3m_p^2}{2\sqrt{s-4m_p^2}}, \\ x_F &= \frac{s_1-s_2-2t_2-2t_1}{s-4m_p^2}. \end{aligned} \tag{3.10}$$

By taking $s,\ s_1,\ s_2 \gg t_1,\ t_2,\ m_p^2,\ m_2^2$ and keeping $\mu = \frac{s_1 s_2}{s}$ fixed, one finds

$$\begin{aligned} sx_F &\approx s_1 - s_2, \\ s_1 &\approx \frac{1}{2}\left[sx_F + \sqrt{s^2x_F^2+4s\mu}\right], \\ s_2 &\approx \frac{1}{2}\left[-sx_F + \sqrt{s^2x_F^2+4s\mu}\right], \\ E_2 &= \frac{s_1+s_2-2m_p^2}{2\sqrt{s}} \approx \frac{\sqrt{s}}{2}\sqrt{x_F^2+4\frac{\mu}{s}}, \end{aligned} \tag{3.11}$$

as well as

$$p_{1\perp}^2 \approx -\frac{t_1}{2}\left(2+x_F-\sqrt{x_F^2+4\frac{\mu}{s}}\right) - \frac{m_p^2}{4}\left(x_F-\sqrt{x_F^2+4\frac{\mu}{s}}\right), \tag{3.12}$$

$$p_{3\perp}^2 \approx -\frac{t_2}{2}\left(2-x_F-\sqrt{x_F^2+4\frac{\mu}{s}}\right) - \frac{m_p^2}{4}\left(x_F+\sqrt{x_F^2+4\frac{\mu}{s}}\right). \tag{3.13}$$

Hence

$$\mathrm{d}(p_{1\perp})^2\mathrm{d}(p_{3\perp})^2 \approx (1-|x_F|)\mathrm{d}t_1\mathrm{d}t_2, \tag{3.14}$$

and

$$|p_{3z}E_1 - p_{1z}E_3| \approx \frac{s}{2}(1-|x_F|). \tag{3.15}$$

The full cross section in the Regge limit is then given by

$$\sigma \approx \frac{1}{2^6(2\pi)^4 s^2} \int \frac{|\overline{\mathcal{A}}|^2}{\sqrt{x_F^2 + 4\frac{\mu}{s}}} \mathrm{d}x_F \mathrm{d}\theta_{13} \mathrm{d}t_1 \mathrm{d}t_2 \tag{3.16}$$

with

$$s_1 \approx s_2 \approx \sqrt{s\mu}, \; p_{1,3_\perp} \approx \sqrt{-t_{1,3}}, \tag{3.17}$$

$$\mu \approx m_2^2 - t_1 - t_2 + 2\sqrt{t_1 t_2}\cos\theta_{12}. \tag{3.18}$$

One can now exploit that the phase space has a sharp peak around $x_F = 0$ in the Regge limit and integrate out the x_F dependence. This yields

$$\sigma \approx \frac{1}{4(4\pi)^4 s^2} \int |\overline{\mathcal{A}}|^2 \ln\left(\frac{s}{\mu}\right) \mathrm{d}\theta_{13} \mathrm{d}t_1 \mathrm{d}t_2. \tag{3.19}$$

3.2 Differential cross section for pseudoscalar meson production

The amplitude for the process given in figure 3.2 is

$$\mathcal{A} = (\bar{u}_1 \Gamma^{\mu\rho} u_a) \Delta_{\mu\rho\kappa\lambda} V^{\kappa\lambda\alpha\beta} \Delta_{\alpha\beta\nu\sigma} (\bar{u}_3 \Gamma^{\nu\sigma} u_b). \tag{3.20}$$

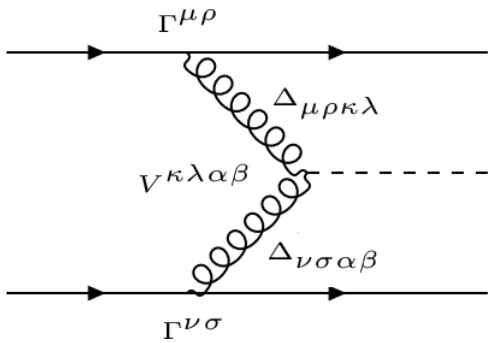

Figure 3.2: Feynman amplitude for CEP of a (pseudo-)scalar meson

This can be simplified using the high energy limit for spinors

$$\bar{u}_{\lambda'}(p')\gamma^\mu u_\lambda(p) \to (p'+p)^\mu \delta_{\lambda\lambda'}, \tag{3.21}$$

which gives, omitting the scalar parts of the propagators,

$$\mathcal{A} \sim \frac{A(t_1)A(t_2)\lambda_p^2}{4}(\epsilon^{\alpha\beta\gamma\delta}(p_1+p_a)_\alpha(p_3+p_b)_\beta(p_a-p_1)_\gamma(p_b-p_3)) \\ ((p_1p_b)(\kappa_a - 4\kappa_b(p_3p_a)) + (p_1p_3)(4\kappa_b)(p_ap_b) + \kappa_a) + \kappa_a(p_3+p_a+p_ap_b))\,, \tag{3.22}$$

for the Sakai-Sugimoto model.

Let $|\overline{\mathcal{A}}|^2$ be the spin averaged amplitude squared then

$$|\overline{\mathcal{A}}|^2 = \frac{1}{4}\sum_{\{s\}}|\mathcal{A}|^2 \tag{3.23}$$

and in the Regge limit one obtains

$$|\overline{\mathcal{A}}|^2 = s^4 t_1 t_2 \sin^2\theta_{13}(\kappa_a - \kappa_b\cos\theta_{13}\sqrt{t_1t_2})^2 A(t_1)^2 A(t_2)^2\lambda_p^4 \times \ldots \tag{3.24}$$

where the dots represent the propagators. This yields the observed $\sin\theta_{13}^2$ dependence.

The normalized differential cross section has then been fitted to the experimental data from WA102 using the reggeized form of the propagators. Additionally the process has been calculated using the propagators and the $\mathbb{P}pp$ vertex from the Tensor-Pomeron model. The results are shown in figure 3.3 and 3.4.

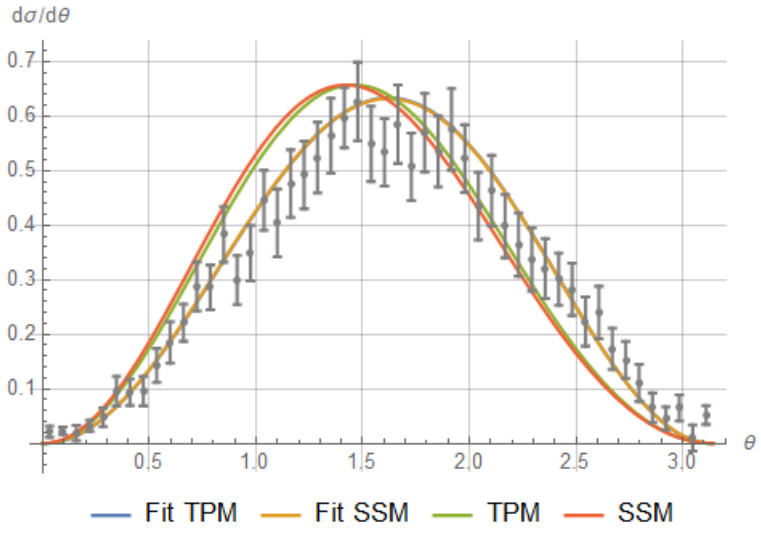

Figure 3.3: Experimental data and Sakai-Sugimoto model predictions for η' meson production. Propagators and $\mathbb{P}pp$ vertices from the Sakai-Sugimoto model as well as from the Tensor-Pomeron model have been used.

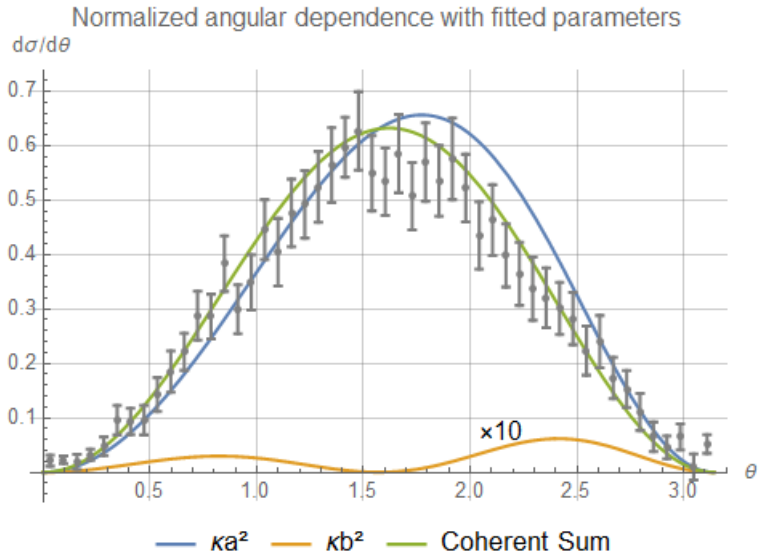

Figure 3.4: Different contributions of the fitted coupling constants of eq. (3.26) using string reggeization. The κ_b^2 contribution has been enhanced by a factor of 10 for better visibility.

Due to different normalization conventions for the pomeron propagators, only the ratio of the coupling constants can be calculated using fitting procedures. The Sakai-Sugimoto model predicts a fraction of[2]

$$\frac{\kappa_a}{\kappa_b} = -0.46 \tag{3.25}$$

whereas from the fit one obtains

$$\frac{\kappa_a}{\kappa_b} = -1.13 \pm 0.12, \tag{3.26}$$

which is in quite good agreement. Note that the fit suggests a stronger coupling to the $(l, S) = (1, 1)$ component, leading to the conclusion that the dominant contributions are due to lower spin excitations on the Regge trajectory.

3.3 Differential cross section for axial vector meson production

The amplitude for the process given in figure 3.5 is now

$$\mathcal{A} = (\bar{u}_1 \Gamma^{\mu\rho} u_a) \Delta_{\mu\rho\kappa\lambda} V^{\gamma\kappa\lambda\alpha\beta} \Delta_{\alpha\beta\nu\sigma} (\bar{u}_3 \Gamma^{\nu\sigma} u_b) \varepsilon_\gamma(\lambda_2) \tag{3.27}$$

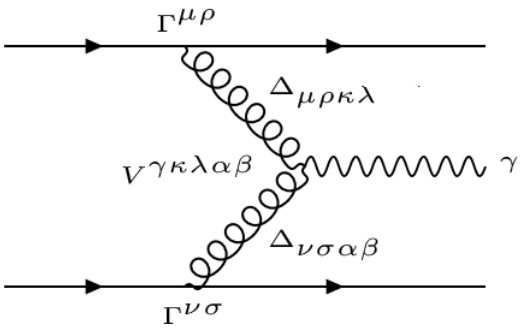

Figure 3.5: Feynman amplitude for CEP of an axial vector meson

[2]The exact numerical values are currently being checked, so this result is not final. See the upcoming publication for the exact values.

Again using the high energy limit for spinors (3.21) and omitting the scalar parts of the propagator gives

$$\begin{aligned}\mathcal{A} \sim & \frac{3}{8} A(t_1)A(t_2)\lambda_p^2 \epsilon^{\alpha\beta\gamma\delta}(p_1+p_a)_\beta(p_3+p_b)_\gamma p_{2\delta}\varepsilon_\alpha(\lambda_2) \\ & ((p_1p_b)(\kappa_c-\kappa_d(p_3p_a))+(p_1p_3)(4\kappa_d(p_ap_b)+\kappa_c)+\kappa_c(p_3p_a+p_ap_b))\end{aligned} \tag{3.28}$$

Squaring the amplitude, averaging over initial state spins and summing over final state spins gives in the Regge limit

$$\begin{aligned}|\overline{\mathcal{A}}|^2 = & A(t_1)^2A(t_2)^2\lambda_p^4 s^4 \left(\kappa_c - \kappa_d \cos^2\theta_{13}\sqrt{t_1t_2}\right)^2 \\ & \frac{4t_1t_2\sin^2\theta_{13} - 2m_2^2\cos^2\theta_{13}\sqrt{t_1t_2} - m_2^2(t_1+t_2)}{4m_2^2} \times \dots\end{aligned} \tag{3.29}$$

where the dots represent the propagators and the polarization sum for massive vector particles

$$\sum_{\lambda_2=0,\pm} \varepsilon_\alpha(\lambda_2)\varepsilon_{\alpha\prime}(\lambda_2) = -g_{\alpha\alpha\prime} + \frac{p_{2\alpha}p_{2\alpha\prime}}{m_2^2} \tag{3.30}$$

has been used.

As before, using the reggeized form of the propagators, the differential cross section has then been fitted to the experimental data from WA102. Additionally the process has been calculated using the propagators and the $\mathbb{P}pp$ vertex from the Tensor-Pomeron model. The results are show in figure 3.6 and 3.7.

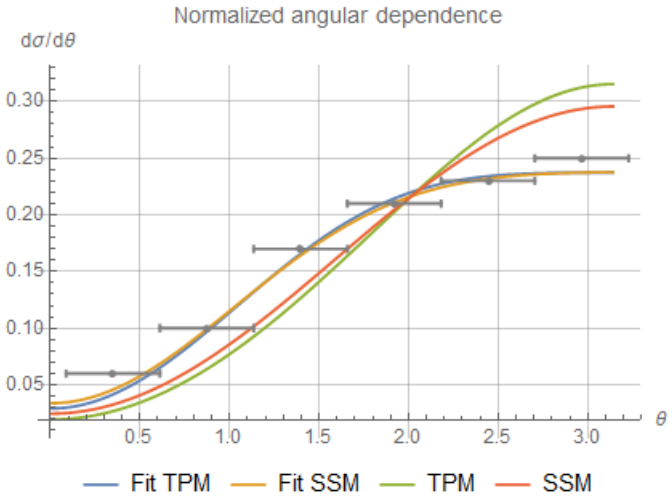

Figure 3.6: Experimental data and Sakai-Sugimoto model predictions for f_1 meson production. Propagators and vertices from the Sakai-Sugimoto model as well as from the Tensor-Pomeron model have been used.

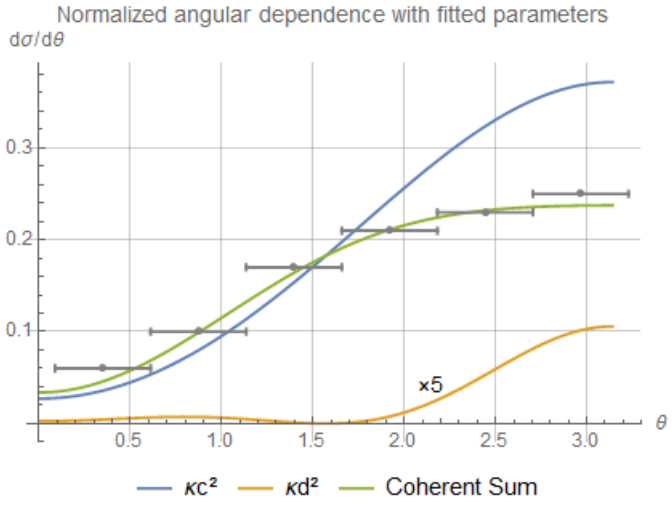

Figure 3.7: Different contributions of the fitted coupling constants of eq. (3.32) using string reggeization. The κ_d^2 contribution has been enhanced by a factor of 5 for better visibility.

The ratio of the coupling constants predicted by the Sakai-Sugimoto model is given by[3]

$$\frac{\kappa_c}{\kappa_d} = -3.2 \tag{3.31}$$

whereas from the fit one obtains

$$\frac{\kappa_c}{\kappa_d} = -0.64 \pm 0.06. \tag{3.32}$$

This suggests that higher lying spins on the pomeron trajectory couple more strongly.

The $g'_{\mathbb{PP}f1}$ and κ_c vertices from the Tensor-Pomeron model and Sakai-Sugimoto model do not fully agree at the Lagrangian level , which gives a non-vanishing contribution in the Regge limit. The difference arising through this term is shown in figure 3.8. Since the mismatch is rather small it will be hard to detect.

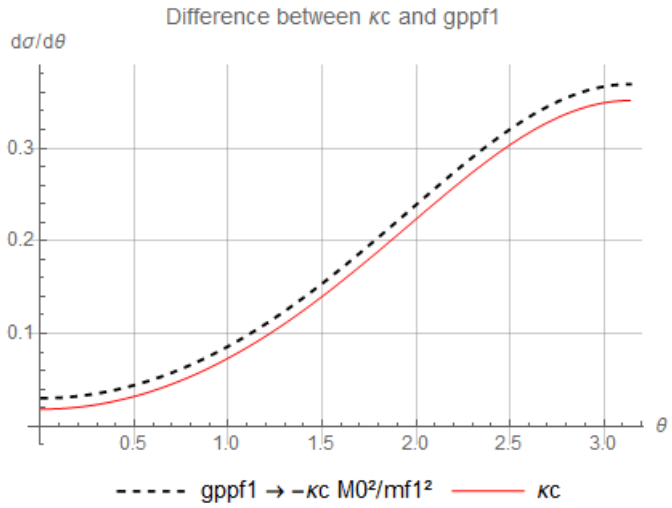

Figure 3.8: Difference between $g'_{\mathbb{PP}f_1}$ and κ_c coupling terms.

[3]The exact numerical values are currently being checked, so this result is not final. See the upcoming publication for the exact values.

The couplings $g'_{\mathbb{P}\mathbb{P}f1}$ and $g''_{\mathbb{P}\mathbb{P}f1}$ have also been fitted to experimental data which gives

$$\frac{g'_{\mathbb{P}\mathbb{P}f1}}{g''_{\mathbb{P}\mathbb{P}f1}} = -0.156 \pm 0.03. \tag{3.33}$$

In figure 3.9 the resulting differential cross section is plotted for each coupling separately as well as their coherent sum which leads to destructive interference.

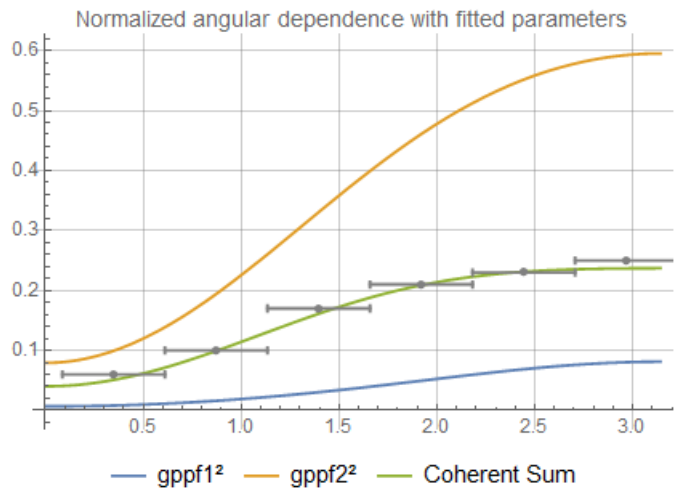

Figure 3.9: Predictions from the Tensor-Pomeron model with fitted couplings to WA102 data.

3.4 Further possible couplings

Now the additional interactions of equations (2.72g)-(2.72h) with no counterparts in the previous models will be studied.

When the amplitude is contracted with the vertices and propagators of figure 3.5 and squared, the V_7 vertex gives a vanishing contribution.

The V_8 vertex however gives the non vanishing result

$$|\overline{\mathcal{A}}|^2 = \kappa_e^2 s^4 t_1 t_2 \sin\theta_{13}^2 (2\cos\theta_{13}\sqrt{t_1 t_2} - t_1 - t_2) \frac{m_{f1}^2 + 2\cos\theta_{13}\sqrt{t_1 t_2} - t_1 - t_2}{4m_{f1}^2} \times \dots \tag{3.34}$$

in the Regge limit, resulting in the differential cross section of figure 3.10, where TPM propagators and the $\mathbb{P}pp$ vertex as well reggeized string propagators have been used.

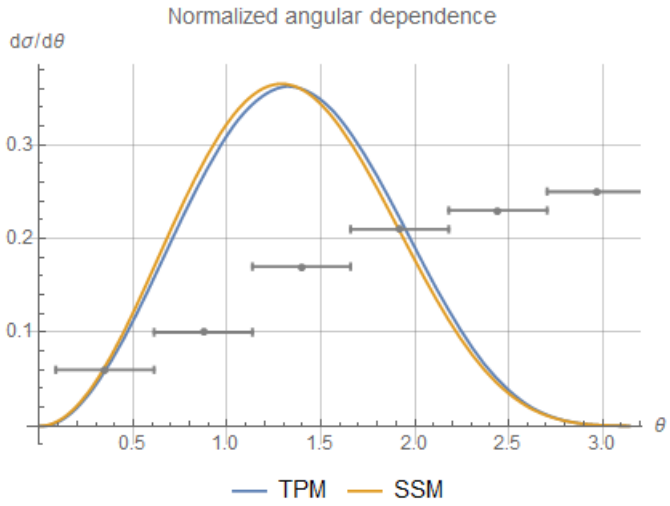

Figure 3.10: Contribution of V_8 coupling to the differential cross section.

Chapter 4

Conclusions and outlook

In this thesis it was shown that the Sakai-Sugimoto model as well as the Tensor-Pomeron model give identical results regarding the tensorial structure of the vertices for pseudoscalar meson production but with different form factors. However, the former seems to underestimate the coupling strengths to Pomerons. Including meson exchange by considering reggeons to improve the results was done in Ref.[24] by Anderson et al. and produced only a slightly better agreement. However, due to work from Dickson et al. [38] and Domokos et al. [39], they came to the conclusion that the Witten-Sakai-Sugimoto model systematically underestimates coupling constants.

Glueballs are still elusive in experiments but central exclusive production remains one of the most promising methods of detecting glueball candidates [40]. Hence, calculating further interaction terms coupling glueballs to mesons is an interesting topic for future work in the Tensor-Pomeron model as well as the Witten-Sakai-Sugimoto model.

Acknowledgements

I would like to thank Anton Rebhan for giving me the chance to take part in this exciting research project and supervising this thesis. I wish to acknowledge the help provided by Josef Leutgeb for his assistance with the Mathematica code and hints for improving it as well as many useful discussions. Furthermore I would like to thank my dear friend Lukas Gosch for sharing his knowledge on fitting procedures and for all the insightful discussions we have had regarding my studies at the university as well as outside. Lastly I would like to thank my parents, Petra and Roland Hechenberger, for their support and encouragement throughout university and beyond.

Appendices

Appendix A

Tables of numerical values

Table of numerical values used for Sakai-Sugimoto model calculations

All the values are taken from [33] and [35]. If not stated otherwise, the values are predictions from Sakai-Sugimoto model calculations

λ_P	9.02 GeV^{-1}	
α'_c	0.290 Gev^{-2}	Fitted value using pp scattering
m_g	1.485 GeV	
κ_a	-0.172 GeV^{-1}	
κ_b	0.372 GeV^{-3}	
κ_c	12.399	
κ_d	-3.864 GeV^{-2}	
M_D	1.17 GeV	

Table A.1: Sakai-Sugimoto model parameters

Table of numerical values used for Tensor-Pomeron model calculations

All the values are taken from [22] and [23]. If not stated otherwise, the values are obtained from fits to experimental data.

$\beta_{\mathbb{P}NN}$	1.87 GeV^{-1}	
$\alpha'_{\mathbb{P}}$	0.25 GeV^{-2}	
$\epsilon_{\mathbb{P}}$	0.0808	
M_D	0.84 GeV	
μ_p/μ_N	2.7928	Theoretical prediction
$g'_{\mathbb{PP}\eta'}$	2.61	
$g''_{\mathbb{PP}\eta'}$	1.5	

Table A.2: Tensor-Pomeron model parameters

List of masses

Masses taken from [15].

m_p	0.938 GeV
$m_{\eta'}$	0.958 GeV
m_{f1}	1.285 GeV
m_π	0.135 GeV

Table A.3: Masses used for calculations

Non-linear Regge trajectory parameters

δ	0.08009
α_1	0.298
α_2	0.02467

Table A.4: Fitted parameters for the Regge trajectory in equation (2.74) from [36].

Appendix B

Chiral symmetry breaking and the η' mass

For a comprehensive treatment of the subject see e.g. [41].

B.1 Chiral symmetry

Consider a $SU(N_c)$ gauge theory coupled to N_f massless fermions

$$\mathcal{L} = -\frac{1}{2g^2}\mathrm{Tr}G_{\mu\nu}G^{\mu\nu} + \sum_{i=1}^{N_f} i\bar{\psi}_i \not{D}\psi_i \tag{B.1}$$

where $\not{D}\psi = \not{\partial}\psi - i\not{A}\psi$. The fermionic Lagrangian can be decomposed into left and right handed Weyl fermions and thus the theory has a global $G_f = U(N_f)_L \times U(N_f)_R = U(1)_V \times SU(N_f)_L \times SU(N_f)_R$ chiral symmetry. The theory is thought to lead to the formation of a (chiral) quark condensate which is supported by lattice simulations

$$\langle \bar{\psi}_{Li}\psi_{Rj}\rangle = -\sigma U_{ij}, \tag{B.2}$$

where σ is a constant of mass dimension three and $U_{ij} \in SU(N_f)$. The formation of this condensate leads to the breaking of the global G_f symmetry with pattern

$$G_f = U(1)_V \times SU(N_f)_L \times SU(N_f)_R \to U(1)_V \times SU(N_f)_V. \tag{B.3}$$

The unbroken $SU(N_f)_V$ subgroup stems from the fact that (B.2) remains invariant if $L = R$. The theory now contains $N_f^2 - 1$ Goldstone bosons which can be parametrized by

$$U(x) = \exp\left(\frac{2i}{f_\pi}\pi(x)\right), \quad \pi(x) = \pi^a(x)T^a, \tag{B.4}$$

with T^a being the $su(N_f)$ generators. For $N_f = 2$ the theory contains three of these bosons: $\pi^0\pi^\pm$. From this one can obtain a low-energy effective action with Lagrangian

$$\mathcal{L}_{ch} = \frac{f_\pi^2}{4}\,\mathrm{Tr}\left(\partial^\mu U^\dagger \partial_\mu U\right) \tag{B.5}$$

which is of the type of the non-linear sigma models of chapter 1.1.

According to Noether's theorem, there are associated currents to the $SU(N_f)_L \times SU(N_f)_R$ chiral symmetry which are parametrized by

$$\begin{aligned} J^a_{V\mu} &= J^a_{L\mu} + J^a_{R\mu} = \overline{\psi}_i T^a_{ij}\gamma_\mu\psi_j \\ J^a_{A\mu} &= J^a_{L\mu} - J^a_{R\mu} = \overline{\psi}_i T^a_{ij}\gamma_\mu\gamma^5\psi_j. \end{aligned} \tag{B.6}$$

Considering an infinitesimal expansion of

$$L = e^{i\alpha^a T^a} = 1 + i\alpha^a T^a + \mathcal{O}(\alpha^2) \tag{B.7}$$

and

$$\begin{aligned} &\alpha^a \to \alpha^a(x) \\ &\delta\mathcal{L} = \partial_\mu\alpha^a(x) J^{a\mu}_L. \end{aligned} \tag{B.8}$$

in the chiral Lagrangian (B.5) yields the current as

$$J^a_{L\mu} \approx -\frac{f_\pi}{2}\partial_\mu\pi^a \tag{B.9}$$

and analogously

$$J^a_{R\mu} \approx +\frac{f_\pi}{2}\partial_\mu\pi^a \tag{B.10}$$

Including masses in the theory

$$\mathcal{L} = -\frac{1}{2g^2}\mathrm{Tr}G_{\mu\nu}G^{\mu\nu} + \sum_{i=1}^{N_f}(i\overline{\psi}_i \not{D}\psi_i - m_i\overline{\psi}_i\psi_i) \tag{B.11}$$

explicitly breaks the chiral symmetry. However, the main contribution to the breaking still comes from the chiral condensate, so eq. (B.2) is now to be understood in an approximate sense. By introducing the mass matrix

$$M = \mathrm{diag}(m_1, \ldots, m_{N_f}) \tag{B.12}$$

the chiral Lagrangian (B.5) can now be rewritten as

$$\mathcal{L}_{ch} = \frac{f_\pi^2}{4}\mathrm{Tr}\left(\partial^\mu U^\dagger \partial_\mu U\right) + \frac{\sigma}{2}\mathrm{Tr}\left(MU + U^\dagger M^\dagger\right) \tag{B.13}$$

and expanding $U = e^{2i\pi/f_\pi}$ in this action yields a mass term for the pions

$$\mathcal{L}_{ch} \approx \mathrm{Tr}(\partial^\mu \pi \partial_\mu \pi) - \frac{\sigma}{f_\pi^2}\mathrm{Tr}(M + M^\dagger)\pi^2. \tag{B.14}$$

The observed meson masses are however significantly larger than the masses of their constituent quarks as what would the simple expansion of the chiral Lagrangian for $N_f = 2$ suggest. The main contribution stems from the interaction of the sea quarks and gluons, i.e. one should consider the renormalised masses in the chiral Lagrangian.

B.2 The light pseudoscalar mesons

For the three lightest quarks u, d and s, which are almost of the same order of magnitude of mass and significantly lighter than the other quarks and assuming an exact $SU(3)$ flavour symmetry, one would expect eight pseudoscalar Goldstone bosons

$$\pi = \frac{1}{\sqrt{2}}\begin{pmatrix} \frac{\pi^0}{\sqrt{2}} + \frac{\eta}{\sqrt{2}} & \pi^+ & K^+ \\ \pi^- & -\frac{\pi^0}{\sqrt{2}} + \frac{\eta}{\sqrt{2}} & K^0 \\ K^- & \overline{K}^0 & -\frac{2\eta}{\sqrt{6}}. \end{pmatrix} \tag{B.15}$$

There are however nine pseudoscalar mesons with only u, d and s valence quark content. This ninth pseudoscalar meson is associated with the breaking of the so called axial symmetry.

B.3 The $U(1)_A$ symmetry and the Witten-Veneziano formula

The ninth pseudoscalar meson is the $\eta' = \frac{1}{\sqrt{3}}(u\overline{u} + d\overline{d} + s\overline{s})$ which is a singlet under $SU(3)_V$ and corresponds to the Goldstone boson associated to the $U(1)_A$ symmetry. The $U(1)_A$ symmetry is however broken by an anomaly and the η' is significantly more massive than the other pseudoscalar mesons

of the broken chiral symmetry.

Considering the change of the path integral measure and associating it with the corresponding Noether current one finds

$$\partial_\mu J^\mu_A = \frac{\lambda N_f}{8\pi^2 N_c} \mathrm{Tr} F_{\mu\nu} \tilde{F}^{\mu\nu}, \tag{B.16}$$

where $\tilde{F}$ is the dual field strength, thus the anomaly will be suppressed by $1/N_c$ in the 't Hooft limit $N_c \to \infty$ and $\lambda = g^2 N_c$ fixed, restoring the full chiral symmetry of YM theory coupled to massless fermions. Note that the right hand side of eq. (B.16) is proportional to the CP violating θ term. So by defining the topological susceptibility

$$\chi(k) = \int \mathrm{d}^4 x e^{ikx} \langle 0| \mathrm{Tr}(\tilde{F}_{\mu\nu} F^{\mu\nu}(x)) \mathrm{Tr}(\tilde{F}_{\rho\sigma} F^{\rho\sigma}(0)) |0\rangle , \tag{B.17}$$

which gives the response to the energy of the system by varying θ since

$$\frac{\mathrm{d}^2 E}{\mathrm{d}\theta^2} = \left(\frac{1}{16\pi^2 N_c} \right)^2 \lim_{k\to 0} \chi(k), \tag{B.18}$$

one can relate the ground state energy to the mass of the η' meson. Perturbative calculations at leading order in $1/N_c$ of $\chi(k)$ lead to vanishing results as $k \to 0$, however summing the infinite series is expected to give a non-vanishing result [41]. This can schematically be done in the large N_c limit as follows: Consider an arbitrary glueball operator

$$\mathcal{G}(x) = \mathrm{Tr} F^m(x), \tag{B.19}$$

with $m \geq 2$ and take the connected two-point function

$$\langle 0| \tilde{\mathcal{G}}(k) \tilde{\mathcal{G}}(-k) |0\rangle_c , \tag{B.20}$$

By identifying this two-point function with tree-level propagation of single particle states, it can be expanded in terms of propagating single particle glueball states $|n\rangle$ with amplitude $a_n = \langle 0| \mathcal{G}(x) |n\rangle$ and mass M_n

$$\langle 0| \tilde{\mathcal{G}}(k) \tilde{\mathcal{G}}(-k) |0\rangle_c = \sum_n \frac{|a_n|^2}{k^2 - M_n^2}. \tag{B.21}$$

this identification is diagrammatically shown in figure B.1.

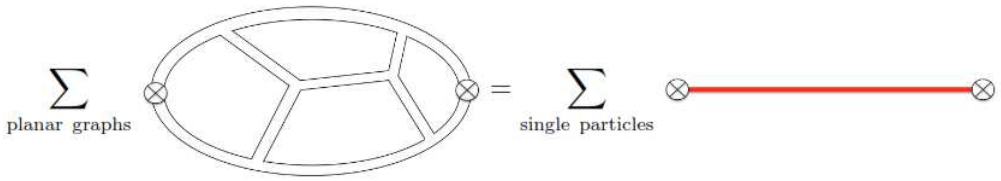

Figure B.1: Replacement of connected two-point functions in the large N_c limit. Image from [41].

Analogously for mesons with meson operator

$$\mathcal{J}(x) = \sqrt{N_c}\bar{\psi}F^m(x)\psi, \tag{B.22}$$

with m arbitrary. The normalisation factor is chosen such that the connected two-point function $\langle 0|\,\mathcal{J}\mathcal{J}\,|0\rangle_c \sim N_c^0$ has the correct amplitude in the large N_c limit. The connected two-point functions with single particle meson states $|n\rangle$ of mass m_n and with amplitudes $b_n = \langle 0|\,\mathcal{J}(x)\,|n\rangle$ is then given by

$$\langle 0|\,\tilde{\mathcal{J}}(k)\tilde{\mathcal{J}}(-k)\,|0\rangle_c = \sum_n \frac{|b_n|^2}{k^2 - m_n^2}. \tag{B.23}$$

Continuing this schematic approach, quantities like the energy $E(\theta)$ or the susceptibility $\chi(k)$ will receive contributions of the form [42]

$$\langle 0|\,\mathrm{Tr}\tilde{F}F\,|n^{\mathrm{th}}glueball\rangle = N_c a_n,\ \langle 0|\,\mathrm{Tr}\tilde{F}F\,|n^{\mathrm{th}}meson\rangle = \sqrt{N_c}b_n. \tag{B.24}$$

due to planar graphs made from gluons and planar graphs including quark lines.
In the massless theory, the θ dependence must vanish since the chiral symmetry is then exact. For this to happen, the contribution to the susceptibility from the glueball states must cancel the contribution from the meson states which are however of unequal order of magnitude in N_c. So schematically

$$\chi(k) = \sum_{\mathcal{G}} \frac{N_c^2|a_n|^2}{k^2 - M_n^2} + \sum_{\mathcal{M}} \frac{N_c|b_n|^2}{k^2 - m_n^2}, \tag{B.25}$$

where $\mathcal{G}$ and $\mathcal{M}$ denote the glueball and meson states, respectively. For the vacuum, i.e. the limit $k \to 0$, these terms ought to cancel. But in order to do so, a meson whose mass scales as $m^2 \sim 1/N_c$ is needed. Assuming the η' behaves as such, one can conclude that

$$\chi(0)|_{YM} = \frac{N_c b_{\eta'}^2}{m_{\eta'}^2} \tag{B.26}$$

and using eq.(B.16) to write

$$\sqrt{N_c} b_{\eta'} = \langle 0| F\tilde{F} |\eta'\rangle = \frac{8\pi^2 N_c}{\lambda N_f} \langle 0| \partial_\mu J_A^\mu |\eta'\rangle = -i\frac{8\pi^2 N_c}{\lambda N_f} p^\mu \langle 0| J_A^\mu |\eta'\rangle . \tag{B.27}$$

For the chiral Lagrangian (B.5) it was found that $\langle 0| J_A^\mu |\eta'\rangle = -i\sqrt{N_f} f_\pi p_\mu$ with a factor of $\sqrt{N_f}$ to give the correct normalization and make f_π independent of N_f. Hence

$$b_{\eta'} = \frac{8\pi^2\sqrt{N_c}}{\sqrt{N_f}\lambda} f_\pi m_{\eta'}^2 \tag{B.28}$$

and using eq.(B.18) one finally obtains

$$m_{\eta'}^2 = \frac{4N_f}{f_\pi^2} \frac{\mathrm{d}^2 E}{\mathrm{d}\theta^2}|_{\theta=0}, \tag{B.29}$$

which is known as the Witten-Veneziano formula. It relates the mass of the η' meson to the vacuum energy of large N_c YM theory.

Appendix C

Additional Information on the Pomeron

In this section the pomeron is constructed from QFT principles and Regge theory as in Ref.[22]. Due to the QFT approach it is possible to formulate a Lagrangian which couples the pomeron to the proton and antiproton, respectively. The Pomeranchuk theorem [43], which states that under certain assumptions the cross sections for a collision of a particle and the corresponding antiparticle on the same target approach the same value at high energies, is shown to hold for this construction. Furthermore it is shown how the pomeron can be interpreted as a Regge trajectory with even spins starting at $J = 2$. This derivation is closely following [22].

C.1 The $\mathbb{P}pp$ vertex

Consider pp and $p\overline{p}$ elastic scattering

$$\begin{aligned} p(p_1) + p(p_2) &\to p(p_1') + p(p_2') \\ \overline{p}(p_1) + p(p_2) &\to \overline{p}(p_1') + p(p_2)' \end{aligned} \tag{C.1}$$

with kinematic variables

$$\begin{aligned} s = (p_1 + p_2)^2,\ t = (p_1 - p_1')^2,\ u = (p_1 - p_2')^2 \\ \nu = \frac{1}{4}(s - u) = \frac{1}{4}(p_1 + p_1')(p_2 + p_2'). \end{aligned} \tag{C.2}$$

The spinor structure $\Gamma_{\alpha,\alpha',\beta,\beta'}$ of the $\mathcal{T}$ matrix elements can now be expanded in the basis $\{\gamma^\mu, \gamma^5, \mathbb{I}\} \otimes \{\gamma_\mu, \gamma_5, \mathbb{I}\}$. Whilst crossing symmetry requires

$$\Gamma^{\bar{p}p}_{\alpha,\alpha',\beta,\beta'}(p_1',p_2',p_1,p_2) = -\Gamma^{pp}_{\alpha,\alpha',\beta,\beta'}(-p_1,p_2',-p_1',p_2), \tag{C.3}$$

the assumption that only a vector like structure contributes to pomeron exchange in the high energy limit [44] gives

$$\begin{aligned}\Gamma^{pp}_{\alpha,\alpha',\beta,\beta'}(p_1',p_2',p_1,p_2) &= T^{pp}(\nu,t)(\gamma^\mu)_{\alpha\alpha'}(\gamma_\mu)_{\beta\beta'},\\ \Gamma^{\bar{p}p}_{\alpha,\alpha',\beta,\beta'}(p_1',p_2',p_1,p_2) &= T^{\bar{p}p}(\nu,t)(\gamma^\mu)_{\alpha\alpha'}(\gamma_\mu)_{\beta\beta'}.\end{aligned} \tag{C.4}$$

For fixed t, T^{pp} and $T^{\bar{p}p}$ are boundary values of one analytic function in ν, $A(\nu,t)$. This relates to the fact that due to crossing symmetry amplitudes of different physical processes are equivalent. The amplitude $A(\nu,t)$ now has branch points with cuts attached to them at ν_1 and ν_2 with $\nu_1 < \nu_2$. In the interval $\nu_1 < \nu < \nu_2$ the amplitude is real and following the analysis of chapter 2.1 one finds for $\nu > \nu_2$

$$\begin{aligned}T^{pp}(\nu,t) &= \lim_{\epsilon\to 0} A(\nu+i\epsilon,t),\\ T^{\bar{p}p}(\nu,t) &= -\lim_{\epsilon\to 0} A(-\nu-i\epsilon,t).\end{aligned} \tag{C.5}$$

Assuming a power behaviour for $A(\nu,t)$ and making an ansatz with odd powers for $\nu\to\infty$ (corresponding to a $C=+1$ exchange since the pomeron has vacuum quantum numbers; see eq.C.5) to give the same amplitudes for pp and $\bar{p}p$ scattering the ansatz for the pomeron part of the amplitude reads

$$A^{\mathbb{P}}(\nu,t) = \underbrace{[3\beta_{\mathbb{P}NN}F_1(t)]^2}_{f(t)}\, 2\alpha'_{\mathbb{P}}\nu[4\alpha'^2_{\mathbb{P}}(\nu_2-\nu)(\nu-\nu_1)]^{\frac{1}{2}(\alpha_{\mathbb{P}}(t)-2)} \tag{C.6}$$

Using now equation (C.5) one can show that

$$T^{pp\mathbb{P}}(\nu,t) = T^{\bar{p}p\mathbb{P}}(\nu,t) = f(t)2\alpha'_{\mathbb{P}}\nu[4\alpha'^2_{\mathbb{P}}\nu^2 e^{-i\pi}]^{\frac{1}{2}(\alpha_{\mathbb{P}}(t)-2)}, \tag{C.7}$$

as expected from the pomeranchuk theorem. In the high energy limit $\nu\approx\frac{s}{2}$ and equation (C.6) reduces to the Donnachie-Landshoff pomeron ansatz

$$A^{\mathbb{P}}(\nu,t) = [3\beta_{\mathbb{P}NN}F_1(t)]^2(-is\alpha'_{\mathbb{P}})^{\alpha_{\mathbb{P}}(t)-1}. \tag{C.8}$$

Note that this result is purely obtained from QFT results combined with regge theory. Due to the $\gamma^\mu\times\gamma_\mu$ structure of the $\mathcal{T}$ matrix element, the pomeron is sometimes viewed as a $C=+1$ photon, which is in contradiction with the total cross sections of pp and $\bar{p}p$ elastic scattering having the same sign. However the above construction enables one to view the pomeron as

an effective $J = 2$ exchange with the right crossing requirements. Take for example the high energy limit of the reactions (C.1)

$$\begin{aligned}
&\langle p(p_1', \lambda_1'), p(p_2', \lambda_2')|\, \mathcal{T}\, |p(p_1, \lambda_1), p(p_2, \lambda_2)\rangle\, |_{\mathbb{P}} \\
&= \langle \overline{p}(p_1', \lambda_1'), p(p_2', \lambda_2')|\, \mathcal{T}\, |\overline{p}(p_1, \lambda_1), p(p_2, \lambda_2)\rangle\, |_{\mathbb{P}} \\
&= i2s[3\beta_{\mathbb{P}NN} F_1(t)]^2 (-is\alpha_{\mathbb{P}}')^{\alpha_{\mathbb{P}}(t)-1} \delta_{\lambda_1,\lambda_1'} \delta_{\lambda_2,\lambda_2'}.
\end{aligned} \tag{C.9}$$

To construct a suitable interaction Lagrangian, consider the following ansatz which couples a symmetric and traceless rank two tensor object to the proton and antiproton

$$\mathcal{L}_{\mathbb{P}pp} = -3\beta_{\mathbb{P}NN} \mathbb{P}_{\mu\nu} \frac{i}{2} \overline{\psi}_p \left[\gamma^\mu \overleftrightarrow{\partial}^\nu + \gamma^\nu \overleftrightarrow{\partial}^\mu - \frac{1}{2} g^{\mu\nu} \gamma^\lambda \overleftrightarrow{\partial}_\lambda \right] \psi_p. \tag{C.10}$$

Using the ansätze from the Tensor-Pomeron model for the propagator (2.38) and the resulting vertex from the interaction Lagrangian (C.10) yields equation (C.9) in the high energy limit. Which shows that eq. (C.10) is a suitable effective Lagrangian.

C.2 The pomeron as coherent sum of spin 2,4,... exchanges

The pomeron is usually viewed as a coherent sum of spin exchanges [45]. In the following section this property is also shown to hold for the Tensor-Pomeron model.
Considering the amplitude for elastic pp scattering and using (C.7) gives

$$\begin{aligned}
&\langle p(p_1'), p(p_2')|\, \mathcal{T}\, |p(p_1), p(p_2)\rangle\, |_{\mathbb{P}} \\
=& f(t) \exp\left[-i\pi \frac{1}{2} (\alpha_{\mathbb{P}}(t) - 2) \right] (4\alpha_{\mathbb{P}}'^2 v^2)^{\frac{1}{2}(\alpha_{\mathbb{P}}(t)-2)} 2\alpha_{\mathbb{P}}' \nu \\
&\times \overline{u}(p_1')\gamma^\mu u(p_1) \overline{u}(p_2')\gamma_\mu u(p_2) = \mathcal{T}_{if}^{\mathbb{P}}.
\end{aligned} \tag{C.11}$$

Recall that

$$\nu = \frac{1}{4}(p_1 + p_1')(p_2 + p_2') \tag{C.12}$$

and rewrite parts of the expression using

$$(4\alpha_{\mathbb{P}}'^2\nu^2)^{\frac{1}{2}(\alpha_{\mathbb{P}}(t)-2)} = \frac{1}{\Gamma(1-\frac{1}{2}\alpha_{\mathbb{P}}(t))}\int_0^\infty \mathrm{d}\tau\tau^{-\frac{1}{2}\alpha_{\mathbb{P}}(t)}\exp\bigl(-4\alpha_{\mathbb{P}}'^2\nu^2\tau\bigr) \tag{C.13}$$

gives

$$\mathcal{T}_{if}^{\mathbb{P}} = \tilde{f}(t)\int_0^\infty \mathrm{d}\tau\tau^{-\frac{1}{2}\alpha_{\mathbb{P}}(t)}\exp\bigl(-4\alpha_{\mathbb{P}}'^2\nu^2\tau\bigr)2\alpha_{\mathbb{P}}'\nu\overline{u}(p_1')\gamma^\mu u(p_1)\overline{u}(p_2')\gamma_\mu u(p_2) \tag{C.14}$$

with

$$\tilde{f}(t) = f(t)\exp\left[-i\pi\frac{1}{2}(\alpha_{\mathbb{P}}(t)-2)\right]\Gamma\left(1-\frac{1}{2}\alpha_{\mathbb{P}}(t)\right)^{-1}. \tag{C.15}$$

Making a series expansion for the exponential and using the high energy limit for spinor products with gamma matrices

$$(p'+p)^\mu\delta_{\lambda\lambda'} \to \overline{u}_{\lambda'}(p')\gamma^\mu u_\lambda(p) \tag{C.16}$$

to replace ν given by eq. (C.12) yields

$$\begin{aligned}\mathcal{T}_{if}^{\mathbb{P}} = \tilde{f}(t)\int_0^\infty \mathrm{d}\tau\tau^{-\frac{1}{2}\alpha_{\mathbb{P}}(t)}\sum_{n=1}^\infty\frac{(-\tau)^{n-1}}{(n-1)!}\left(\frac{1}{2}\alpha_{\mathbb{P}}'\right)^{2n-1}\\ \times\overline{u}(p_1')R^{\mu_1\cdots\mu_{2n}}(p_1',p_1)u(p_1)\overline{u}(p_2')R_{\mu_1\cdots\mu_{2n}}(p_2',p_2)u(p_2),\end{aligned} \tag{C.17}$$

where

$$\begin{aligned}R^{\mu_1\cdots\mu_{2n}}(p',p) = \frac{1}{2n}\{&\gamma^{\mu_1}(p'+p)^{\mu_2}\cdots(p'+p)^{\mu_{2n}} + (p'+p)^{\mu_1}\gamma^{\mu_2}\cdots(p'+p)^{\mu_{2n}}\\ &+\cdots+(p'+p)^{\mu_1}\cdots(p'+p)^{\mu_{2n-1}}\gamma^{\mu_{2n}}\}.\end{aligned} \tag{C.18}$$

Thus $\mathcal{T}_{if}^{\mathbb{P}}$ has been rewritten as a coherent sum of even spin exchanges starting at spin two. Note that in this procedure an index shift has been performed to combine the powers of $2\alpha_{\mathbb{P}}'\nu$ from the exponential and the rest of the integrand and thus the sum starts at $n=1$ rather than $n=0$, which would correspond to a scalar pomeron exchange.

Appendix D

Heuristic derivation of meson fields in the Witten-Sakai-Sugimoto model

As already mentioned in the main text, this appendix should only highlight some key features which are necessary to reflect intrinsic properties of QCD such as chiral symmetry breaking. For additional information see [3] and [26].

In Ref.[4] it was shown that the near horizon geometry obtained from certain compactifications of M-Theory where the fourth spatial coordinate (i.e. Kaluza-Klein direcetion) is compactified using

$$x_4 + 2\pi R_4 \equiv x_4 + 2\pi M_{KK}^{-1} \backsimeq x_4 \tag{D.1}$$

with supersymmetry breaking boundary conditions is given by

$$\mathrm{d}s^2 = \left(\frac{u}{R}\right)^{3/2} \left[\eta_{\mu\nu}\mathrm{d}x^\mu \mathrm{d}x^\nu + f(u)\mathrm{d}x_4^2\right] + \left(\frac{R}{u}\right)^{3/2} \left[\frac{\mathrm{d}u^2}{f(u)} + u^2 \mathrm{d}\Omega_4^2\right] \tag{D.2}$$

with

$$f(u) = 1 - \frac{u_{KK}^3}{u^3}, \quad M_{KK} = \frac{3}{2}\frac{u_{KK}^{1/2}}{R^{3/2}} \tag{D.3}$$

and $u \geq u_{KK}$ being the holographic direction with $u = \infty$ corresponding to the conformal boundary, dilaton $e^\phi = g_s(u/R)^{3/4}$ and R being the spacetime curvature radius.

The gravity action can now be written as

$$S_{grav} = \frac{1}{2\kappa_{10}^2}\int \mathrm{d}^{10}x\sqrt{-g}\left[e^{-2\phi}\left(R + 4(\nabla\phi)^2 - \frac{(2\pi)^4 l_s^2}{2\cdot 4!}F_4^2\right)\right] \tag{D.4}$$

with

$$F_4 = \mathrm{d}C_3 = \frac{2\pi N_c}{V_4}\epsilon_4 \tag{D.5}$$

and l_s being the string tension. C_3 is the Ramond-Ramond 3-form, ϵ_4 the volume form and $V_4 = 8\pi^2/3$ the volume of a unit S_4. The supersymmetry breaking boundary conditions are given by a thermal circle in Euclidean time τ

$$\tau \equiv \tau + \frac{2\pi}{M_{KK}}. \tag{D.6}$$

This now leads to a confined phase

$$\begin{aligned} \mathrm{d}s^2 =& \left(\frac{u}{R}\right)^{3/2}[\mathrm{d}\tau^2 + \mathrm{d}\mathbf{x}^2 + f(u)\mathrm{d}x_4^2] \\ &+ \left(\frac{R}{u}\right)^{3/2}\left[\frac{\mathrm{d}u^2}{f(u)} + u^2\mathrm{d}\Omega_4^2\right] \\ M_{KK} =& \frac{3}{2}\frac{u_{KK}^{1/2}}{R^{3/2}}, \quad f(u) \equiv 1 - \frac{u_{KK}^3}{u^3} \end{aligned} \tag{D.7}$$

and a deconfined phase

$$\begin{aligned} \mathrm{d}s^2 =& \left(\frac{u}{R}\right)^{3/2}[\tilde{f}(u)\mathrm{d}\tau^2 + \mathrm{d}\mathbf{x}^2 + \mathrm{d}x_4^2] \\ &+ \left(\frac{R}{u}\right)^{3/2}\left[\frac{\mathrm{d}u^2}{\tilde{f}(u)} + u^2\mathrm{d}\Omega_4^2\right] T = \frac{3}{4\pi}\frac{u_T^{1/2}}{R^{3/2}}, \quad \tilde{f}(u) \equiv 1 - \frac{u_T^3}{u^3} \end{aligned} \tag{D.8}$$

with Hawking-Page transition when $2\pi T = M_{KK}$. The topologies in the (τ, u) and (x_4, u) subspaces, respectively, are given in figure D.1.

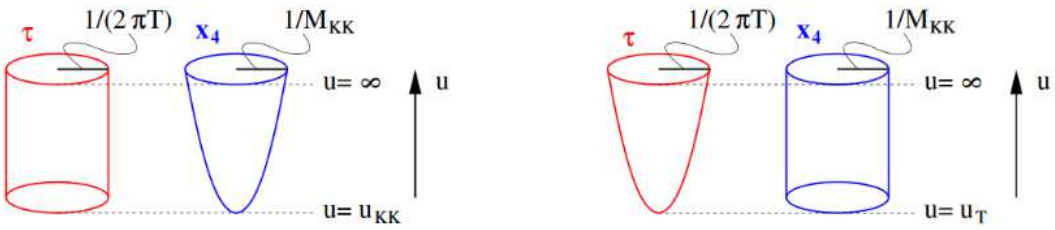

Figure D.1: Topologies of the confined (left) and deconfined (right) phase. The cigar topology in the (x_4, u) subspace in the confined phase becomes a Euclidean black hole in the (τ, u) subspace of the deconfined phase. Image taken from [46].

In Ref.[3] Sakai and Sugimoto now added D8 and anti-D8 flavor branes filling all spatial directions except the x_4 to the configuration to account for chiral quarks. Open strings connecting those D-Branes carry a color index and a second index which can be identified with the flavor quantum number. The result of intersecting color and flavor branes are chiral quarks. The configuration is shown in figure D.2a. The D8 and anti D8 branes can only join in the bulk (see figure D.2b) since they have nowhere to end. This spontaneously breaks the $U(N_f)_L \times U(N_f)_R$ gauge symmetry on the flavour branes.

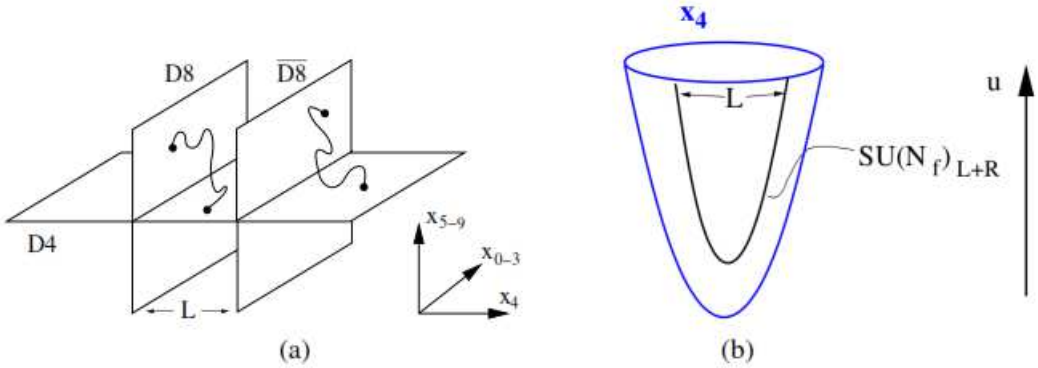

Figure D.2: (a) Configuration of the D4,D8 and $\overline{\text{D8}}$ branes including open strings which can be identified as chiral quarks. (b) Near-horizon geometry with u being a radial coordinate in the transverse space $x_5 \ldots_9$. Image taken from [26].

The action on the D8 brane is given to leading order in N_c and α' by

$$S_{\mathrm{D8}} = -\kappa \int \mathrm{d}^4x \mathrm{d}Z \mathrm{Tr}\left[\frac{1}{2}(1+Z^2)^{-1/3}F_{\mu\nu}^2 + (1+Z^2)M_{KK}^2 F_{\mu Z}^2 + \mathcal{O}(\alpha'^2 F^4)\right] + S_{CS},$$
$$\kappa = \frac{g^2 N_c^2/2}{216\pi^3}, \tag{D.9}$$

where

$$\left(\frac{u}{u_{KK}}\right)^3 = 1 + Z^2, \ -\infty < Z < \infty \tag{D.10}$$

and the Chern-Simons term can be shown to reproduce the correct chiral anomaly of QCD [3]

$$S_{CS} = T_8 \int_{D8} C \wedge \mathrm{Tr}\left[\exp\left(\frac{F}{2\pi}\right)\right]\sqrt{\hat{A}(\mathcal{R})}. \tag{D.11}$$

Making an ansatz for normalizable modes in D.9

$$A_\mu(x^\mu, Z) = \sum_{n=1}^{\infty} v_\mu^n(x^\mu)\psi_n(Z), \quad A_Z(x^\mu, Z) = -i\pi(x^\mu)\phi_0(Z) \tag{D.12}$$

and choosing the ψ_n such that they satistfy

$$-(1+Z^2)^{-1/3}\partial_Z\left((1+Z^2)\partial_Z\psi_N\right) = \lambda_n\psi_n, \quad m_n^2 = \lambda_n M_{KK}^2, \tag{D.13}$$

in order to get the correct normalizations in the resulting effective action for open string excitations in the Witten background, gives

$$S = S_{D8} + S_{CS} = -\mathrm{Tr}\int \mathrm{d}^4x \left[\frac{1}{2}(\partial_\mu\pi)^2 + \frac{1}{4}F_{\mu\nu}^2 + \frac{1}{2}\lambda_1 M_{KK}^2\rho_\mu^2 + \cdots\right]. \tag{D.14}$$

This action includes states that can be identified with π and ρ mesons. In Ref.[31] it was then shown that glueball states can be identified with metric fluctuations resulting from the linearized Einstein equations about the $\mathrm{AdS}_7\times S^4$ black hole background, which has been sketched in chapter 2.3.

Bibliography

[1] Asner, D. M. *et al.* Physics at BES-III. *arXiv:0809.1869 [hep-ex, physics:hep-lat, physics:hep-ph]* (2008). 0809.1869.

[2] Collaboration, P. *et al.* Physics Performance Report for PANDA: Strong Interaction Studies with Antiprotons. *arXiv:0903.3905 [hep-ex]* (2009). 0903.3905.

[3] Sakai, T. & Sugimoto, S. Low energy hadron physics in holographic QCD. *Progress of Theoretical Physics* **113**, 843–882 (2005). hep-th/0412141.

[4] Witten, E. Anti-de Sitter Space, Thermal Phase Transition, And Confinement In Gauge Theories. *arXiv:hep-th/9803131* (1998). hep-th/9803131.

[5] Hashimoto, K., Tan, C.-I. & Terashima, S. Glueball Decay in Holographic QCD. *Phys. Rev. D* **77**, 086001 (2008). 0709.2208.

[6] Brünner, F., Parganlija, D. & Rebhan, A. Holographic Glueball Decay. *Acta Phys. Pol. B Proc. Suppl.* **7**, 533 (2014). 1407.6914.

[7] Klempt, E. & Zaitsev, A. Glueballs, Hybrids, Multiquarks. Experimental facts versus QCD inspired concepts. *Physics Reports* **454**, 1–202 (2007). 0708.4016.

[8] Gupta, R. Introduction to Lattice QCD. *arXiv:hep-lat/9807028* (1998). hep-lat/9807028.

[9] Salpeter, E. E. & Bethe, H. A. A Relativistic Equation for Bound-State Problems. *Phys. Rev.* **84**, 1232–1242 (1951).

[10] Kim, Y., Shin, I. J. & Tsukioka, T. Holographic QCD: Past, Present, and Future. *Progress in Particle and Nuclear Physics* **68**, 55–112 (2013). 1205.4852.

[11] Parganlija, D., Kovacs, P., Wolf, G., Giacosa, F. & Rischke, D. H. Meson vacuum phenomenology in a three-flavor linear sigma model with (axial-)vector mesons. *Phys. Rev. D* **87**, 014011 (2013). 1208.0585.

[12] Scherer, S. Introduction to Chiral Perturbation Theory (2002).

[13] Morningstar, C. J. & Peardon, M. The glueball spectrum from an anisotropic lattice study. *Phys. Rev. D* **60**, 034509 (1999).

[14] Sanchis-Alepuz, H., Fischer, C. S., Kellermann, C. & von Smekal, L. Glueballs from the Bethe-Salpeter equation. *arXiv:1503.06051 [hep-lat, physics:hep-ph, physics:hep-th]* (2015). 1503.06051.

[15] Tanabashi, M. *et al.* Review of Particle Physics. *Phys.Rev.* **D98**, 030001 (2018).

[16] Kirk, A. WA102 proposal talk (1995).

[17] http://www.ep.ph.bham.ac.uk/exp/WA102/layout.html. WA102 1995 Layout.

[18] Kirk, A. A review of central production experiments at the CERN Omega spectrometer. *Int. J. Mod. Phys. A* **29**, 1446001 (2014). 1408.1196.

[19] Donnachie, S., Dosch, H. G., Nachtmann, O. & Landshoff, P. Pomeron physics and QCD. *Camb.Monogr.Part.Phys.Nucl.Phys.Cosmol.* **19**, 1–347 (2004).

[20] Collins, P. D. B. An Introduction to Regge Theory and High-Energy Physics (2009).

[21] Lehmann, H. Il Nuovo Cimento **10**, 579 (1958).

[22] Ewerz, C., Maniatis, M. & Nachtmann, O. A Model for Soft High-Energy Scattering: Tensor Pomeron and Vector Odderon. *Annals of Physics* **342**, 31–77 (2014). 1309.3478.

[23] Lebiedowicz, P., Nachtmann, O. & Szczurek, A. Exclusive central diffractive production of scalar and pseudoscalar mesons; tensorial vs. vectorial pomeron. *Annals of Physics* **344**, 301–339 (2014). 1309.3913.

[24] Anderson, N., Domokos, S. K. & Mann, N. Central production of η via double Pomeron exchange and double Reggeon exchange in the Sakai-Sugimoto model. *Physical Review D* **96**, 046002 (2017).

[25] Nachtmann, O. (Coupling of an f1-type meson to two pomerons, Private communication).

[26] Rebhan, A. The Witten-Sakai-Sugimoto model: A brief review and some recent results. *arXiv:1410.8858 [hep-ph, physics:hep-th, physics:nucl-th]* (2014). 1410.8858.

[27] 't Hooft, G. A Planar Diagram Theory for Strong Interactions. *Nucl.Phys.* **B72**, 461 (1974).

[28] Aharony, O., Gubser, S. S., Maldacena, J., Ooguri, H. & Oz, Y. Large N Field Theories, String Theory and Gravity. *Physics Reports* **323**, 183–386 (2000). hep-th/9905111.

[29] Baggioli, M. A Practical Mini-Course on Applied Holography. *arXiv:1908.02667 [cond-mat, physics:hep-ph, physics:hep-th]* (2019). 1908.02667.

[30] Maldacena, J. M. The Large N Limit of Superconformal Field Theories and Supergravity. *International Journal of Theoretical Physics* **38**, 1113–1133 (1999). hep-th/9711200.

[31] Brower, R. C., Mathur, S. D. & Tan, C.-I. Glueball Spectrum for QCD from AdS Supergravity Duality. *Nuclear Physics B* **587**, 249–276 (2000). hep-th/0003115.

[32] Resonance production in central pp collisions at the CERN Omega Spectrometer. *Physics Letters B* **489**, 29–37 (2000).

[33] Anderson, N., Domokos, S. K., Harvey, J. A. & Mann, N. Central production of η and η' via double Pomeron exchange in the Sakai-Sugimoto model. *Physical Review D* **90**, 086010 (2014).

[34] Domokos, S. K., Harvey, J. A. & Mann, N. The Pomeron contribution to p p and p bar p scattering in AdS/QCD. *Phys. Rev. D* **80**, 126015 (2009). 0907.1084.

[35] Leutgeb, J. (Sakai-Sugimoto model couplings, Private communication).

[36] Szanyi, I., Jenkovszky, L., Schicker, R. & Svintozelskyi, V. Pomeron/glueball and odderon/oddball trajectories. *arXiv:1910.02494 [hep-ph]* (2019). 1910.02494.

[37] Byckling, E. & Kajantie, K. *Particle Kinematics* (Wiley, London, New York, 1973).

[38] Dickson, R. & Schumacher, R. A. Photoproduction of the f1(1285) Meson. *Phys. Rev. C* **93**, 065202 (2016). 1604.07425.

[39] Domokos, S. K., Grigoryan, H. R. & Harvey, J. A. Photoproduction through Chern-Simons term induced interactions in holographic QCD. *Phys. Rev. D* **80**, 115018 (2009).

[40] Guryn, W. Central Exclusive Particle Production in DPE Process: Search for Glueballs etc. *Acta Physica Polonica B* **47**, 53 (2016).

[41] Tong, D. Gauge Theory - Lecture Notes (2018). Http://www.damtp.cam.ac.uk/user/tong/gaugetheory.html.

[42] Mariño, M. Instantons and Large N: An Introduction to Non-Perturbative Methods in Quantum Field Theory (2015).

[43] Pomeranchuk, I. Y. Soviet Physics: Journal of Experimental and Theoretical Physics **7**, 499 (1958).

[44] Landshoff, P. V. & Polkinghorne, J. C. The dual quark-parton model and high energy hadronic processes. *Nuclear Physics B* **32**, 541–556 (1971).

[45] Nachtmann, O. Considerations concerning diffraction scattering in quantum chromodynamics. *Annals Phys.* **209**, 436–478 (1991).

[46] Leutgeb, J. Holographic QCD, Talk given at Strong Group Meeting at TU Wien on 05.15.19 (2019).